Timing Synchronization for an Airborne OFDM System

A Thesis

Presented to the faculty of the School of Engineering and Applied Science

University of Virginia

in partial fulfillment of the requirements for the degree

Master of Science

by

Rui Shang

July 2018

Abstract

Orthogonal Frequency Division Multiplexing (OFDM) is widely used in the digital communication field now, for example, in Long Term Evolution (LTE). This modulation technique has achieved high data rates and increased bandwidth efficiency and robustness in complex environments by separating the channel into narrowband flat fading subchannels. OFDM system requires the orthogonality of each subcarrier keeping to the receiver to recover the data transmitted. Synchronization errors in OFDM would cause intersymbol and intercarrier interference which will defect the orthogonality of each subcarrier. One way to achieve timing synchronization is by performing maximum likelihood functions on existing cyclic prefix of OFDM symbols to form peaks at the start of each symbol. The other way to the acquisition of the timing synchronization is by using training symbols in the transmitted OFDM signal. Both algorithms perform well at very low signal-to-noise ratios (SNR). This thesis extends these two previous ways to acquire more accurate timing synchronization and addresses timing synchronization for an airborne OFDM system including the research for different SNRs, multipath and Doppler frequency offset with different synchronization methods.

Acknowledgements

I would like first to thank my advisor, Prof. Stephen G. Wilson for giving me an opportunity to do research with him and guiding me through my whole graduate program.

I would like to thank Laulima Systems support, under contract to National Spectrum Consortium, for providing me the chance to do this research.

I would like to thank my committee members, Prof. Maite Brandt-Pearce and Prof. Daniel S. Weller for devoting their time to be on my thesis committee.

I would like to thank Dr. Satya Ponnaluri for discussing practical problems in the project with our group which helps us keep improving the result.

I would also like to thank Ruixuan He and Mrugen Deshmukh for all their research contributions.

I am grateful to everyone at the University of Virginia who have taught or supervised me, and to Beth Eastwood-Beatty for helping me throughout the program.

Last but not least, I would like to thank my parents, Xiaoping Shang, Chunyan Shang and all my family members for their constant support and encouragement.

List of Figures

2.1 OFDM basic principles shown in classic form 13

2.2 Waveforms of basic digital modulation, BPSK 14

2.3 Basic signal constellations 14

2.4 QAM signal constellations 15

2.5 Power spectral density of QPSK (4-QAM) signal 17

2.6 Basic multicarrier design 17

2.7 OFDM subcarriers in time domain 19

2.8 OFDM baseband subcarriers 19

2.9 Time characteristics of an OFDM signal with 2096 subcarriers 20

2.10 Cyclic prefix real part in an OFDM symbol (time domain) 21

2.11 Typical OFDM transmitter architecture 23

2.12 Typical OFDM receiver architecture 23

3.1 Multipath transmission 26

3.2 Multipath with different delay spread 27

3.3 High-speed aircraft moving toward base station 28

3.4 Impulse response for a frequency selective channel 30

3.5 Frequency response for a frequency selective channel 30

3.6 Impulse response for a time and frequency selective channel 31

4.1 Observation of length $2N + L$ samples for a complete OFDM symbol with CP . . . 34

4.2 Timing and frequency metrics over AWGN channel 37

4.3 Time-domain structure for the first Schmidl-Cox training symbol 38

4.4 Timing metric and frequency estimation using Schmidl-Cox method 39

4.5 Timing metric and frequency estimation using modified Schmidl-Cox method . . . 40

4.6 Effect of timing metric normalization 41

4.7 Timing metric and frequency estimation using Minn's method 42

4.8 Pilots spaced equally 44

4.9 Comparison of Sandell's method and our proposed method at 5 dB 44

5.1 One OFDM symbol structure with semi-random pilot locations 46

5.2 Perfect timing and imperfect timing constellations 48

5.3 Constellation after compensation 49

5.4 Wrong timing constellation after compensation 50

5.5 Comparison for Sandell's method at different SNR 51

5.6 Comparison for our proposed method at different SNR 52

5.7 Comparison for Schmidl-Cox' method at different SNR 52

5.8 Comparison for Minn's method at different SNR 53

5.9 Multipath results with different methods at 5 dB 54

5.10 Timing results with Doppler offset 55

5.11 RMSE for different methods with single path 57

5.12 RMSE for different methods with two-ray multipath 57

5.13 RMSE for different averaging lengths for Sandell's method 58

List of Tables

3.1 Aircraft speed versus Doppler offset for the system under study 28

Contents

1 Introduction **10**

1.1 Contribution . . . 11

1.2 Organization of thesis . . . 12

2 An Overview of OFDM **13**

2.1 Signal Characteristics . . . 14

2.1.1 QAM signal . . . 14

2.1.2 OFDM baseband properties . . . 18

2.1.3 Peak to average ratio . . . 19

2.2 Cyclic Prefix . . . 20

2.3 OFDM transmission and reception schematic . . . 22

3 Signal Propagation and Channel Model **24**

3.1 Physical models in signal propagation . . . 24

3.1.1 Propagation modes . . . 24

3.1.2 Multipath . . . 25

3.1.3 Doppler 27

3.2 Channel Classification 28

3.2.1 Frequency-Selective channels and Time-Selective channels 29

3.3 Noise 31

4 Timing Synchronization in OFDM 33

4.1 Synchronization using cyclic prefix 33

4.2 Synchronization using training symbols 36

4.2.1 Slight modification of Schmidl-Cox method 39

4.3 Synchronization using modified training symbols 41

4.4 Synchronization at low SNR using pilot information 42

5 Simulation and Results 45

5.1 OFDM system parameters 45

5.2 Timing error effects 46

5.3 QPSK timing results comparison 49

5.3.1 Results at different SNR 49

5.3.2 Results with multipath 53

5.3.3 Results with Doppler offset 55

5.4 RMSE of timing index under different SNR 56

6 Conclusion 59

A Overview of project context for research (S.G. Wilson) 61

Chapter 1

Introduction

Due to the increasing demand in the wireless communication field where growing users desiring higher data rates for various purposes, Orthogonal Frequency-Division Multiplexing (OFDM) technology has been introduced to many communication standards. OFDM is a special case of multicarrier transmission, because it divides available channel bandwidth into a large number of closely-spaced subchannels, over which the frequency-responses appear to be nearly flat if the selected subchannel bandwidth is smaller than the coherence bandwidth of the frequency selective channel. Compared to other communication technologies like Global System for Mobile Communication (GSM), Code Division Multiple Access (CDMA), etc., the advantages of OFDM technology are low-complexity implementation compared to a single-carrier system with equalizer, robustness to the multipath fading channel due to narrowband interference affecting only small percentages of the total subcarriers, high spectral efficiency and the ability to provide flexible transmission bandwidths [2].

The first OFDM schemes were presented by Chang [8] in 1966 and Saltzberg [9] in 1967 using conventional analog circuitry. However, widespread application of OFDM system was not possible until more practical works were done by Weinstein and Ebert [1] and Chang and Gibby [4], Hirosaki [5] and Peled and Ruiz [6]. In 1971, Weinstein and Ebert first showed that Discrete Fourier Transform is a realization of OFDM waveform, thereby eliminating the banks of subcarrier oscillators and coherent demodulators by performing the fast Fourier Transform (FFT) [1].

This technology is now used in most broadband wired and wireless communication systems like Asymmetric Digital Subscriber Lines (ADSL), Long Term Evolution (LTE), wireless local area networks (LANs), digital terrestrial television (DTT), and Wi-Fi since it is an effective solution to intersymbol interference caused by a time-dispersive channel. The diverse use of OFDM systems motivates the critical need for accurate symbol synchronization in time. In this thesis, we will explore the synchronization for an airborne OFDM system which is even a harder case for symbol synchronization and includes all cases in the mentioned applications.

One disadvantage of OFDM systems is that highly linear RF amplifiers are needed. An OFDM signal includes hundreds of independently modulated subcarriers, which can give a large Peak-to-Average Power Ratio (PAPR) when added up coherently. When N signals are added with the same phase, they produce a peak power that is N times the average power [3]. Nonlinear distortion will be induced if the amplifiers cannot meet the peak power requirement. Even when highly linear amplifiers meet all requirement, severe reduction in power efficiency presented due to PAPR. In addition, there are two other drawbacks: one is frequency offsets, created by Doppler shifts or differences between oscillators in the transmitter and receiver, which will reduce orthogonality leading to crosstalk; the other is carrier phase noise, also caused by imperfections between oscillators in each terminal.

1.1 Contribution

The main contribution of this thesis is to compare Sandell's, Schmidl-Cox', Minn's and our proposed method used in synchronizing received OFDM signal based on different channel models. The comparison is made in terms of signal-to-noise ratios (SNRs) and multipath. During the study of each algorithm, this thesis also offers some modifications to improve the performance of original methods. The RMSE at different channel conditions for each method is also provided at the end of this thesis. Besides, the synchronization error effects and complexity of each method are also discussed. A conference paper to deal with synchronization using known information at low SNR is published in *2017 IEEE Military Communications Conference (MILCOM)* [16].

1.2 Organization of thesis

Chapter 2 gives an overview of OFDM. The baseband model and top-level description of an OFDM system are illustrated.

Chapter 3 classifies wireless communication channels. Specific mathematical models for the different channels are shown and discussed here.

Chapter 4 focuses on the timing synchronization in OFDM by illustrating different timing synchronization methods. Modifications are made for some algorithms to improve the performance. Complexity for each method also presented here.

Chapter 5 compares different timing synchronization methods via simulations. It displays the performance of each method under different signal-to-noise ratios and multipath. Moreover, it shows the constellation due to various imperfect timing synchronizations as well.

Chapter 6 concludes the experiments and results presented in this thesis and discusses potential future work.

Chapter 2

An Overview of OFDM

Orthogonal Frequency Division Multiplexing (OFDM) is extensively adopted in modern communication systems. It divides a given channel spectrum into multiple small bandwidth subchannels, or subcarriers, in order to make the original high-speed serial signal to be transmitted in parallel through subchannels. In other words, OFDM system offers a better way to cope with equalization of dispersive slow fading channels.

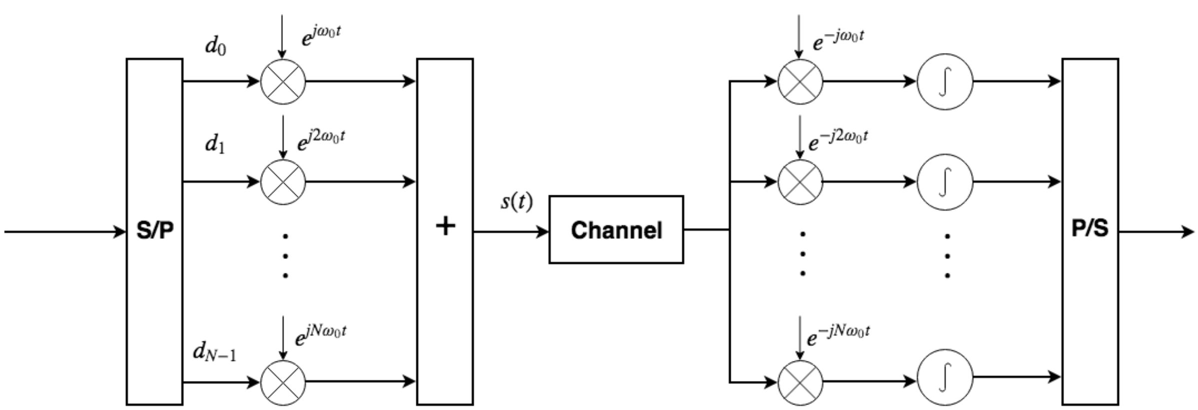

Figure 2.1: OFDM basic principles shown in classic form

The basic model for the original OFDM system is shown in Fig 2.1. As we can see, a serial high-speed data stream is divided into parallel low-rate data streams – each stream is coupled with a known subcarrier or subchannel. Then we add them together and send the sum to the channel. At the receiver, we decouple the signal using the same known subcarrier, then pass them through integrators and serialize the data streams again to get back to the original information.

2.1 Signal Characteristics

2.1.1 QAM signal

In real-time signal transmission, we often use a different combination of sinusoidal waves as transmitting signals. BPSK is one of the most popular binary digital modulation as shown in Fig 2.2.

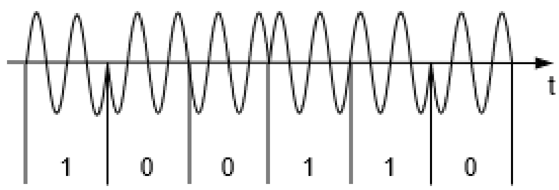

Figure 2.2: Waveforms of basic digital modulation, BPSK

The signal constellation of all possible symbols on a phasor plane is introduced due to its compact and clear way of phasor representation. The constellation of binary PSK are illustrated in Fig 2.3a.

(a) BPSK constellation

(b) 8PSK constellation

Figure 2.3: Basic signal constellations

Higher-order modulations are beneficial because they can describe a large number of possible symbol waveforms. For example, M-ary PSK contains $\log_2 M$ bits per symbol and has M symbol waveforms with different phase angles. Fig 2.3b depicts signal constellation of 8PSK.

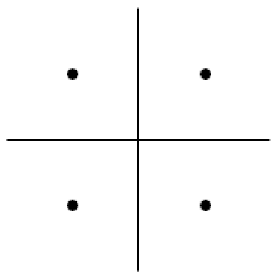

(a) 4QAM constellation

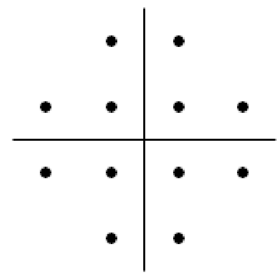

(b) 12QAM constellation

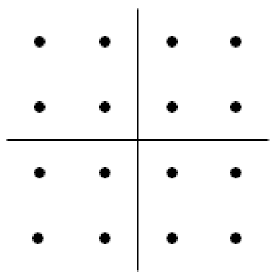

(c) 16QAM constellation

Figure 2.4: QAM signal constellations

Modifying both amplitude and phase in a sinusoidal wave, produces a quadrature amplitude modulation (QAM). QAM is used broadly in digital communication systems, such as Wi-Fi. Here are some examples of 4QAM, 12QAM and 16QAM. As we can see from Fig 2.4, the constellation of 4QAM is exactly the same as 4PSK. In this thesis, the related project in OFDM system design is using 4PSK (4QAM).

We've known M-ary PSK and M-ary QAM are linear modulation systems whose carrier frequency is fixed. In general, the baseband signal for M-ary PSK and M-ary QAM can be expressed as [10]

$$X(t) = \sum_{k=-\infty}^{\infty} (X_I(k) + jX_Q(k))rect(\frac{t}{T} - k) \tag{2.1}$$

where $rect(\cdot)$ is the rectangular pulse with amplitude of 1 between $t = 0$ and $t = 1$ and amplitude of 0 otherwise. $X_I(k)$ and $X_Q(k)$ together form the kth-baseband symbol here which represents the coordinates in the signal constellation.

The auto-correlation function of $X(t)$ can be expressed as[10]

$$\Phi_{XX}(t, t+\tau) = E[x^*(t)x(t+\tau)]$$
$$= E\Big[\sum_{k=-\infty}^{\infty}\sum_{l=-\infty}^{\infty}(X_I(k) - jX_Q(k))(X_I(l) + jX_Q(l)) \cdot rect(\frac{t}{T} - k) \cdot rect(\frac{t+\tau}{T} - k)\Big] \quad (2.2)$$

Then we can average the auto-correlation function by averaging over one period T because $X(t)$ is cyclo-stationary [10]

$$\overline{\Phi_{XX}}(\tau) = \frac{1}{T}\int_0^T \Phi_{XX}(t, t+\tau)dt \quad (2.3)$$

Assume the baseband symbols are independent and are all zero-mean random variable. Let the variance of the baseband symbols be σ^2. Then we have

$$\sigma^2 = E[X_I(0)^2 + X_Q(0)^2] \quad (2.4)$$

Thus, we have [10],

$$\overline{\Phi_{XX}}(\tau) = \begin{cases} \sigma^2(1 - \tau/T), & 0 < \tau < T \\ \sigma^2(1 + \tau/T), & -T < \tau < 0 \\ 0 & \text{otherwise} \end{cases} \quad (2.5)$$

The Fourier transform of above auto-correlation function is the power spectral density of the baseband signal. We then have

$$S_X(f) = \sigma^2 T(\frac{\sin \pi f T}{\pi f T})^2 \quad (2.6)$$

Fig 2.5a and 2.5b show the one-sided power spectral density of QPSK on linear and decibel scale. For single carrier systems, pulse shaping filters are needed since such signals have significant sidelobes which will result in heavy interference to the adjacent frequency band. However, for OFDM systems, pulse shaping filters are only needed after IFFT, before transmission, which is not the case here for M-ary PSK.

Now let's discuss an alternate to single-carrier transmission systems. Parallel transmission systems are favored to make the communication more efficient when the channel frequency response

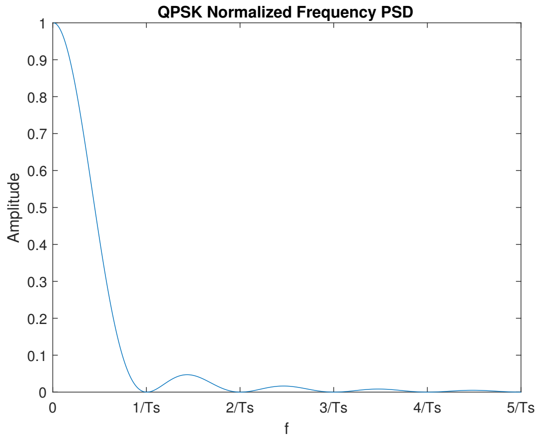

(a) PSD of QPSK signal

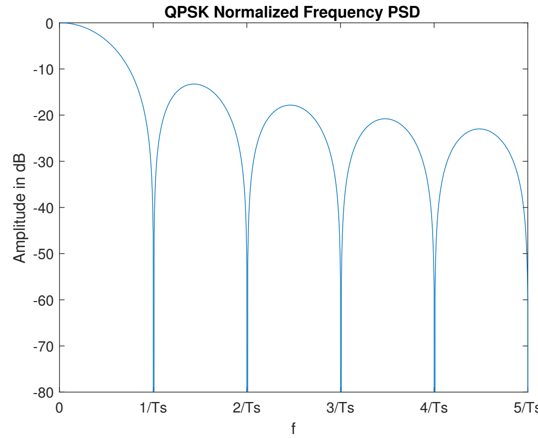

(b) PSD of QPSK in dB

Figure 2.5: Power spectral density of QPSK (4-QAM) signal

varies significantly over the channel bandwidth. In earlier parallel transmission schemes, some non-overlapping signals share the whole available frequency band as shown in Fig 2.6a. Each signal is formed by independent data symbol and transmitted simultaneously with different center frequency. The purpose of the non-overlap is to avoid inter-carrier interference (ICI). But as we can see from the Fig 2.6a, the space between adjacent signals is really a waste of spectrum. Thus, the way of overlapping the signals with different frequencies was introduced from then in Fig 2.6b, which highly improved the spectral efficiency. Based on this overlapping scheme, Orthogonal Frequency Division Multiplexing (OFDM) was developed.

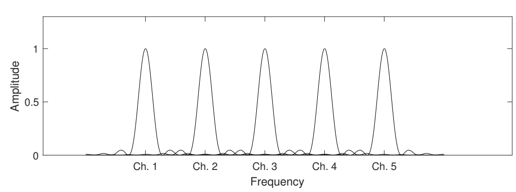

(a) Conventional non-overlapping multicarriers

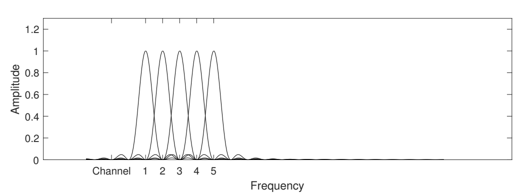

(b) noverlapping multicarriers

Figure 2.6: Basic multicarrier design

2.1.2 OFDM baseband properties

Traditionally, an OFDM signal consists of a set of modulators as in Fig 2.1, each is called a subcarrier and each with different carrier frequencies. Suppose there are N subcarriers modulated by N parallel data streams, which are complex numbers X_k from a given constellation such as QPSK, where $k = 0, 1, ..., N-1$. Also assume f_k is the carrier frequency of kth subcarrier for X_k. Then, we have each baseband subcarrier as

$$\phi_k(t) = e^{j2\pi f_k t} \tag{2.7}$$

The N complex-valued transmitter output for one baseband OFDM symbol (without a cyclic prefix) is

$$s(t) = \sum_{k=0}^{N-1} X_k \phi_k(t) = \sum_{k=0}^{N-1} X_k e^{j2\pi f_k t} \qquad 0 \leq t < NT_s \tag{2.8}$$

where T_s is the sample interval in a digital complementation, and $T = NT_s$ is OFDM symbol interval. To make the subcarriers $\phi_k(t)$ on $0 \leq t < NT_s$ orthogonal, we need equally-spaced subcarrier frequencies f_k:

$$f_k = \frac{k}{NT_s} \tag{2.9}$$

Thus, the subcarrier frequency spacing is now $f_s = \frac{1}{NT}$. The subcarriers of the signal in (2.8) are illustrated in the following Fig 2.7 with index $k = 1, 2, 5$ cases. Fig 2.8 explains how the baseband subcarriers are packed in the frequency domain.

By letting $t = nT_s$, the digital transmitter output is now

$$s(nT_s) = \sum_{k=0}^{N-1} X_k e^{j2\pi f_k nT_s} \qquad 0 \leq nT_s \leq (N-1)T_s \tag{2.10}$$

Then, the OFDM signal is given by

$$s_n = s(nT_s) = \sum_{k=0}^{N-1} X_k e^{j2\pi nk/N} \qquad 0 \leq n \leq N-1 \tag{2.11}$$

From (2.8) we see that the OFDM symbol could be transmitted with different carrier frequencies and be received using a bank of matched filters. However, (2.11) shows when we are

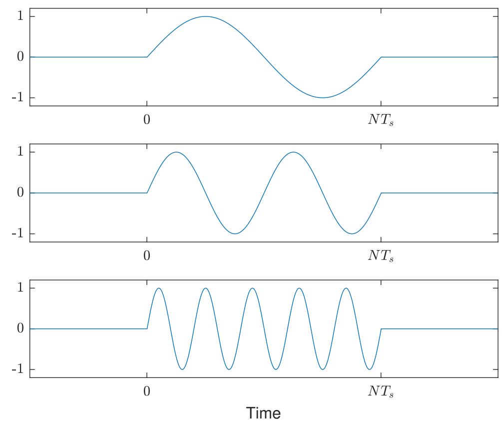

Figure 2.7: OFDM subcarriers in time domain

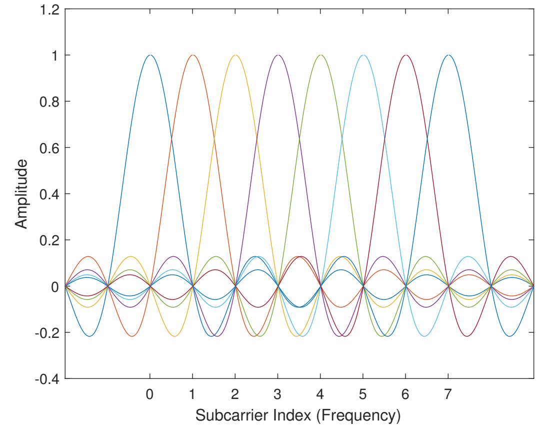

Figure 2.8: OFDM baseband subcarriers

using T_s-spaced sampling of the quadrature and in-phase components of the OFDM symbol, it is the same as we are modulating the sampled data with an inverse discrete Fourier transform (IDFT) except for a multiplying constant coefficient $1/N$. Thus, we don't need a bank of match filters at the receiver. The sampled data will be demodulated with a DFT at the receiver. This is one main property of OFDM first introduced by Weinstein and Ebert [1]. The DFT and IDFT are typically implemented with a Fast Fourier transform (FFT) and Inverse Fast Fourier transform (IFFT) in practical.

Fig 2.9 shows the amplitude of an OFDM symbol with 2096 subcarriers in the time domain and a histogram of its real-part distribution. Since the OFDM signal is the summation of N independent and identically distributed components, the real-part and imaginary-part distribution are roughly Gaussian by central limit theorem [11]. Furthermore, the real and imaginary components are strongly independent, implying the amplitude is a Rayleigh random variable. Thus, OFDM signals have large peak-to-average power ratios. Such large peak-to-average power ratios require amplifiers with high dynamic ranges.

2.1.3 Peak to average ratio

The peak-to-average ratio (PAPR) is the ratio of the peak power to the average power. From the previous section we've seen OFDM systems suffer from high PAPR. The PAPR formula is defined as

$$\text{PAPR} = \frac{\max |s(t)|^2}{E[s(t)^2]} \tag{2.12}$$

The PAPR can reach to maximum of N for N-subcarrier OFDM system in extreme case. The amplifier needs high dynamic range if N is a big number. In order to make the power amplifier work with such large dynamic range, a large output back-off (OBO) must be implemented. The OBO is described as the ratio of output saturation power to the average output power of a power amplifier.

$$\text{OBO(dB)} = 10\log_{10}\frac{P_{o,max}}{P_{o,avg}} \tag{2.13}$$

2.2 Cyclic Prefix

By dividing the serial data stream, which has a rate $1/T_s$, into N subcarriers, the symbol period is then NT_s, each subcarrier is spacing by $1/NT_s$. But real channel time or frequency dispersion (see Chapter 3) can damage the orthogonality between subcarriers which will lead to intercarrier interference (ICI), and in addition, intersymbol interference (ISI) will be introduced by the transmission in dispersive channel. Thus, we need some guard samples to help us reduce ISI and ICI. There are two different ways of inserting some guard period between two successive OFDM symbol. One is inserting all zeros at the beginning, the other is to insert the last tail samples of each OFDM symbol to the beginning which is called **cyclic prefix** (CP). The reason we are

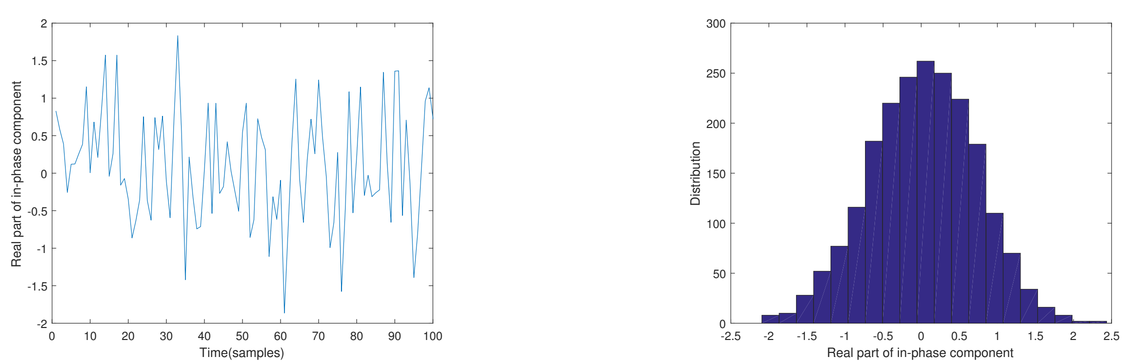

Figure 2.9: Time characteristics of an OFDM signal with 2096 subcarriers

using the cyclic prefix instead of using all zeros is that even both methods can prevent the ISI in a dispersive environment, but only cyclic prefix can maintain orthogonality among subcarriers.

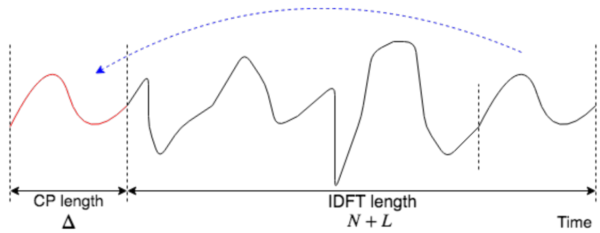

Figure 2.10: Cyclic prefix real part in an OFDM symbol (time domain)

The cyclic prefix, as shown in Fig. 2.10 , is inserted between two consecutive OFDM symbols and extends the OFDM symbol length from N to $N + L$ in samples. The OFDM signal will be passed through a physical channel which is modeled by a finite-length impulse response in$[0, \Delta_h]$. If the impulse response of the channel is longer than the CP time $\Delta = LT_s$, i.e. $\Delta_h > \Delta$, then ISI is introduced. So the CP length should be chosen to have longer duration than the channel impulse response time, $\Delta_h < \Delta$ in OFDM system design.

Besides, we want to do FFT in the receiver to recover the transmitted raw data. Note real channel does regular convolution in continuous time. Thus we have [11]

$$\begin{aligned} r(t) = s(t) * h(t) + w(t) &= \int_0^{\Delta_h} \sum_0^{N-1} X_k e^{j2\pi f_k(t-\tau)} h(\tau) d\tau + w(t) \\ &= \sum_0^{N-1} \Big(\int_0^{\Delta_h} h(\tau) e^{j2\pi f_k(\tau)} d\tau \Big) X_k e^{j2\pi f_k t} + w(t) \\ &= \sum_{k=0}^{N-1} H_k X_k e^{j2\pi f_k t} + w(t) \qquad 0 \le t < NT_s \end{aligned} \tag{2.14}$$

where

$$H_k = \int_0^{\Delta_h} h(\tau) e^{-j2\pi f_k \tau} d\tau \tag{2.15}$$

is the Fourier transform of $h(t)$ evaluated at frequency f_k and $w(t)$ is channel noise. Regular continuous-time convolution in time domain corresponds to multiplication in frequency domain, but not for DFT (or FFT). For DFT, circular convolution in discrete-time domain corresponds to multiplication in discrete frequency domain. Since we want to have multiplication in frequency domain for channel estimation in the following processing, we want circular convolution instead of regular convolution. With CP, regualr convolution can be used to create circular convolution [17]. Discarding the CP sequence to get sampled sequence $y(n)$ at the receiver, and then taking an FFT of the sampled data within $[0, NT_s]$, gets back to the transmitted information X_k by dividing estimated H_k from Y_k:

$$y(n) = s(n) \circledast h(n) + w(n) \tag{2.16}$$

$$Y_k = X_k H_k + W_k \tag{2.17}$$

and equalization,

$$\hat{X}_k = \frac{Y_k}{H_k} \tag{2.18}$$

The disadvantage of cyclic prefix is that it would cause the loss of effective transmission energy and throughput per unit time

$$\varepsilon_{loss} = \frac{NT_s}{NT_s + \Delta} \tag{2.19}$$

This equation also measures the bit rate reduction by CP. In other words, if each subcarrier transmits b bits, then there are Nb bits in every OFDM symbol, the overall bit rate decrease from $\frac{b}{T_s}$ to $\frac{Nb}{NT_s+\Delta}$ after adding CP. The losses can be made very small if we choose the length of the CP Δ much smaller than a symbol period NT_s.

2.3 OFDM transmission and reception schematic

A general OFDM transceiver system is shown in Fig 2.11 and Fig 2.12. As we can see from the figures, the OFDM transmitter integrates several functions, including serial to parallel conversion, inverse FFT processing, CP insertion, pulse shaping filter and digital-to-analog conversion. The OFDM receiver is like the inverse of its transmitter, but it has three additional modules dealing with timing synchronization, channel estimation and channel equalization in order to handle synchronization issues between transmitter and receiver and the channel-fading effect to recover the transmitted data from the noisy channel. The channel effect will be discussed in Chapter 3 and the synchronization issues will be dealt with in Chapter 4. This thesis mainly focuses on symbol timing synchronization part which is marked in yellow in Fig 2.12 since the OFDM system needs to parse a stream of symbols correctly.

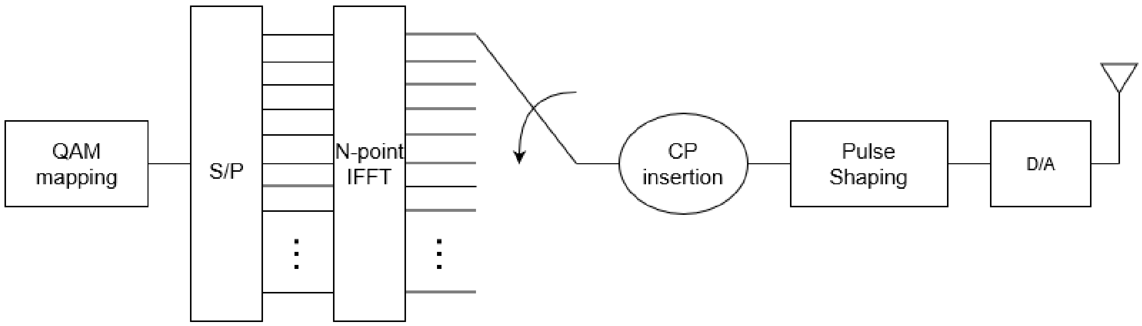

Figure 2.11: Typical OFDM transmitter architecture

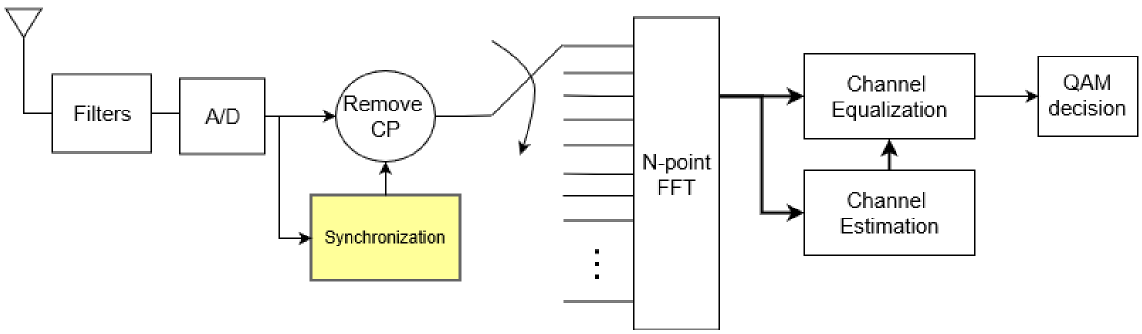

Figure 2.12: Typical OFDM receiver architecture

Chapter 3

Signal Propagation and Channel Model

The study of signal propagation is important to wireless communication since it not only provides the prediction models for the required power estimation, but also helps the receiver to decide how to compensate the impairments due to wireless transmission. In practice, signal propagations may differ based on different environments, but for most cases their physical models are simple in wireless communication.

The propagation effects and other signal impairments are usually collected and directly referred to as the **channel** [18]. The additive white Gaussian noise (AWGN) channel is the most widely used channel model in wireless communication field which we will explain later in this chapter.

3.1 Physical models in signal propagation

3.1.1 Propagation modes

There are three principal propagation modes in wireless communication:

- Free-space propagation, which is related to an ideal situation where path loss is proportional to the square of the distance between the transmitter and receiver. This kind of clear propagation is also called line-of-sight transmission.

- Reflection, which is common to the terrestrial propagation and usually shows greater path loss compared to the free-spaced propagation. It denotes the bouncing of electromagnetic waves from surrounding objects such as walls, mountains, airplanes and cars.

- Diffraction, which is another common terrestrial propagation method. It usually refers to the bending of electromagnetic waves around or through objects like buildings, trees or hills.

The first case is usually described by the free-space link equation. The free-space link equation, also known as the Friis [19] equation, gives the received power as a function of the transmit power P_t, distance d, wavelength λ, antenna gains G_t at the transmitter and G_r at the receiver:

$$P_r = \frac{P_t G_t G_r \lambda^2}{(4\pi d)^2} \quad watts \tag{3.1}$$

This assumes radiation pattern maximums are directed at each other, and that polarizations are matched as explained in [18].

The second and third cases are the cause of the multipath which will be illustrated in the following sections.

3.1.2 Multipath

Due to the reflection and diffraction's impact, the received signal is often the combination of many signals passing through different paths instead of a signal from a line-of-sight transmission. Signals on these different paths may constructively or destructively influence the final signal received at the receiver. In general, when there's more than one path between the transmitter and receiver, we call it multipath. As shown in Fig 3.1, there are two different ways for signal to be transmitted from the transmitter to receiver. One is the direct path, and the other path is caused by the reflection from a building. Usually, the direct path is the dominant path among all paths in

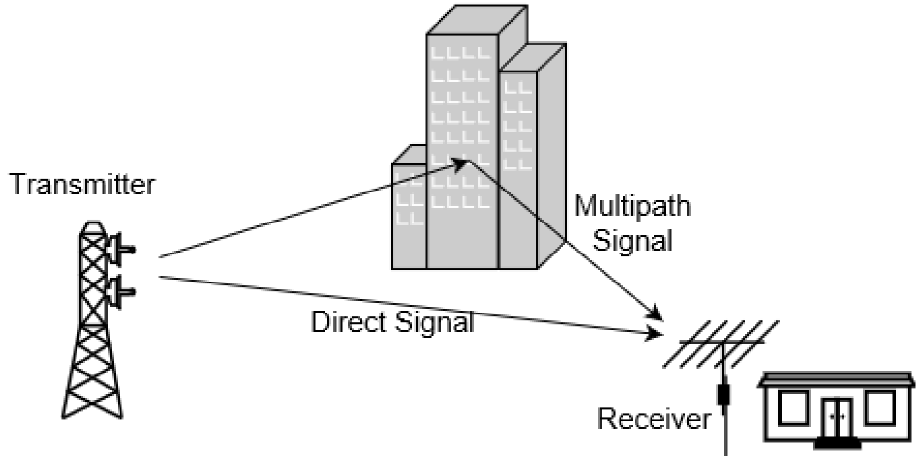

Figure 3.1: Multipath transmission

multipath transmission.

Now consider a simple two-ray propagation. For an unmodulated continuous-wave signal

$$r(t) = \alpha_1 \cos(2\pi f_c t) + \alpha_2 \cos(2\pi f_c (t - \Delta)) \tag{3.2}$$

where α_i are real scale factors, Δ is the differential propagation delay which is also commonly-called the delay spread. Using the complex envelope notation for the received signal, we get

$$\tilde{r}(t) = \alpha_1 + \alpha_2 e^{(-j2\pi f_c \Delta)} \tag{3.3}$$

Thus, we can get the received signal from the above equation enhanced or attenuated based on $f_c\Delta$. The impulse response of this linear two-ray channel is

$$h(t) = \alpha_1 \delta(t) + \alpha_2 \delta(t - \Delta) \tag{3.4}$$

and the channel's frequency response is

$$H(f) = \alpha_1 + \alpha_2 e^{(-j2\pi f \Delta)} \tag{3.5}$$

which is periodic in f with period $1/\Delta$ Hz. Figure 3.2 shows two different two-ray propagations over the bandwidth $B = 1$ MHz, path gain 0.9 and 0.5 for each $\Delta_1 = 1$ μs and $\Delta_2 = 0.15$ μs. As we can see, when the signal spectrum is wider than $1/\Delta$, some frequencies are enhanced and others attenuated, which is called frequency-selective fading. However, if $1/\Delta$ is wider, the channel response is almost a constant which we call flat fading. This is the effect of time dispersion due to multipath.

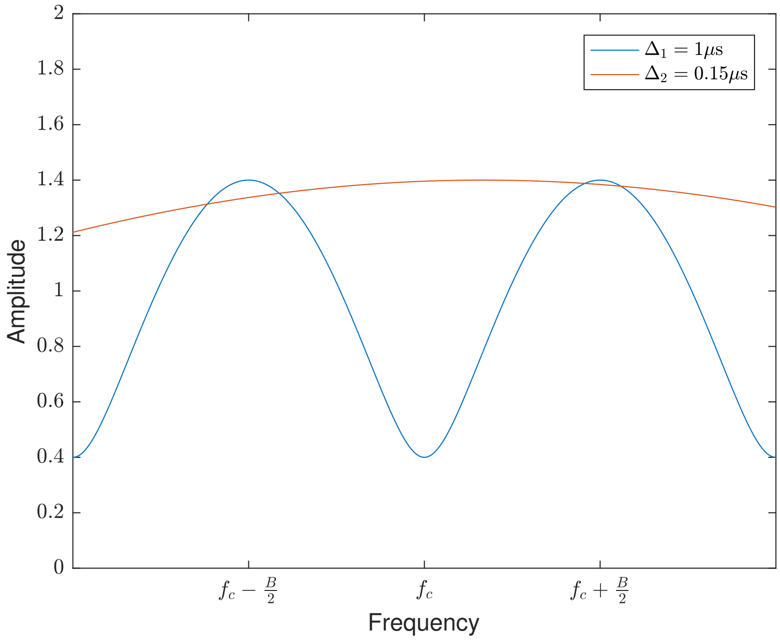

Figure 3.2: Multipath with different delay spread

3.1.3 Doppler

In the previous section, we assumed both terminals are relatively static communicating with each other. But when any one or both terminals are moving, signals are still propagating through those three situations, and the signal itself has changed due to Doppler shift.

Here in Fig 3.3 we are illustrating Doppler with a high-speed aircraft moving toward the base station when sending information from the aircraft to it. Suppose a transmitted signal is $s(t) = A\cos(2\pi f_c t)$, the received signal in a terminal moving at velocity $\vec{v}$ will be

$$r(t) = \alpha_1 A\cos(2\pi(f_c + f_D)(t - t_0)) \tag{3.6}$$

where

$$f_D = \frac{\vec{v} \cdot \vec{u}}{c} \cdot f_c \tag{3.7}$$

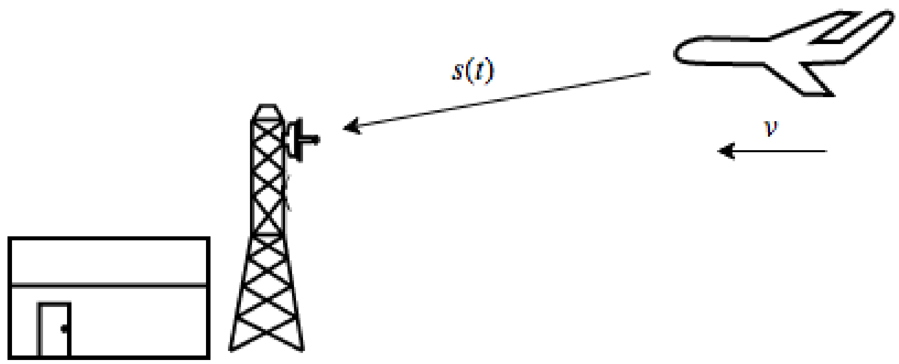

Figure 3.3: High-speed aircraft moving toward base station

and where $\vec{u}$ is a unit vector from the receiver to transmitter. Note the angle between $\vec{u}$ and $\vec{v}$ is between 0° to 180°, so f_D can be positive or negative. Table 3.1 includes some Doppler frequency offsets corresponding to the velocity of the aircraft. For the system under study, the carrier frequency is $f_c = 6$ GHz which can be found in Appendix A. If Doppler frequency offset uncompensated in OFDM, subcarrier orthogonality can be lost.

Aircraft speed	Doppler offset
0 Mach	0 Hz
0.5 Mach	3.313 kHz
1 Mach	6.626 kHz
2 Mach	13.252 kHz
3 Mach	19.878 kHz
50 m/s	1 kHz

Table 3.1: Aircraft speed versus Doppler offset for the system under study

3.2 Channel Classification

In previous sections, we have investigated the effect on received signals based on various propagation phenomena. All those effects can be categorized as large-scale propagation effects and small-scale effects [18]:

- Large-scale effects are due to large objects such as hills, buildings and others. Within an OFDM symbol, these effects varies relatively slowly in time.
- Small-scale effects are due to local environments like trees and nearby buildings which may lead to the reflection, and due to the motion of any terminals. These effects are fast in time. Such effects are often characterized statistically by Rayleigh fading.

We've made the assumption that the channel was linear before. However, the propagation channel may be time-varying. Applying a unit impulse at time $t-\tau$ and then measuring at time t, the shape will change with τ which is represented as a dual-time time-varying impulse response $h(t,\tau)$. For a given signal $s(t)$ to be transmitted in this channel, the output will be:

$$r(t) = \int_{-\infty}^{\infty} h(t,\tau)s(t-\tau)d\tau \tag{3.8}$$

Its baseband equivalent is expressed as:

$$\tilde{r}(t) = \int_{-\infty}^{\infty} \tilde{h}(t,\tau)\tilde{s}(t-\tau)d\tau \tag{3.9}$$

3.2.1 Frequency-Selective channels and Time-Selective channels

First, we develop the modulated received signal when there are N paths:

$$\begin{aligned} r(t) &= \sum_{n=1}^{N} \alpha_n(t)A(t)\cos(2\pi f_c t + \phi(t) + \theta_n(t)) \\ &= \sum_{n=1}^{N} \mathrm{Re}\Big\{\alpha_n(t)e^{j\theta_n(t)}\tilde{s}(t)e^{j2\pi f_c t}\Big\} \end{aligned} \tag{3.10}$$

where $\alpha_n(t)$ is the attenuation and $\theta_n(t)$ is the phase rotation of the nth path.

A frequency-selective channel is a channel with some frequencies enhanced and others attenuated. With large-scale effects, the received signal may include signals from different paths with various path lengths such as the two-ray model in Fig 3.2. The channel response can be

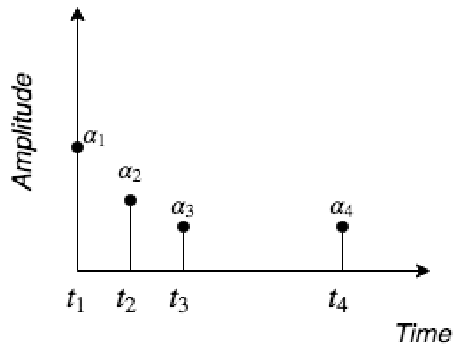

Figure 3.4: Impulse response for a frequency selective channel

represented as following when there are L different paths:

$$\tilde{h}(t,\tau) = \sum_{i=1}^{L} \tilde{\alpha}_i \delta(t - \tau_i) \tag{3.11}$$

where $\tilde{\alpha}_i$ is the complex gain for the i-th path which is $\alpha_i e^{j\theta_i} = \alpha_i e^{-j2\pi f_c \tau_i}$. Figure 3.4 shows the frequency selective channel impulse response with $L = 4$ with delay $\tau_i = 0, 1, 2, 5$ μs and path gain $\alpha_i = 0.9, 0.5, 0.3$ and 0.3. Figure 3.5 gives the amplitude and phase of frequency response in this frequency selective channel.

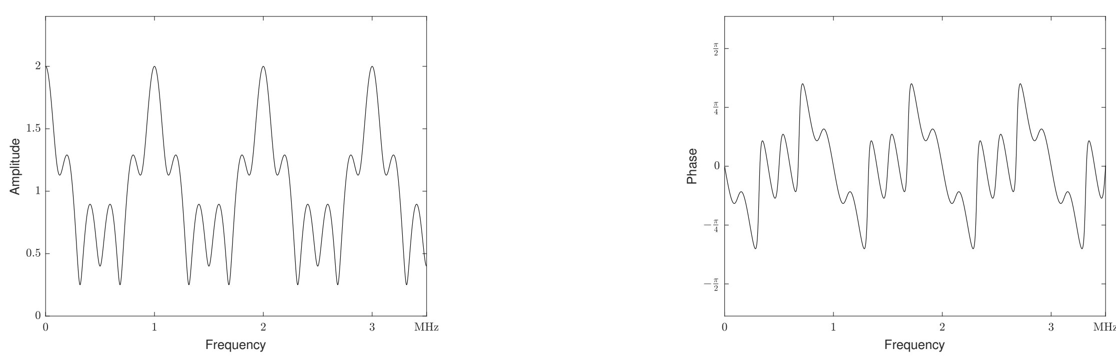

Figure 3.5: Frequency response for a frequency selective channel

A time-selective channel is a channel that changes as a function of time. The channel impuse response is

$$\tilde{h}(t,\tau) = \sum_{i=1}^{L} \tilde{\alpha}_i(t) \delta(t - \tau_i) \tag{3.12}$$

Thus, the received signal power is also changing with time. In other words, in a time-selective channel, the signal received from the channel is sometimes better at a selected time than at other time. Figure 3.6 follows the previous setting with $L = 4$ and shows the channel response of a time-selective and also frequency-selective channel.

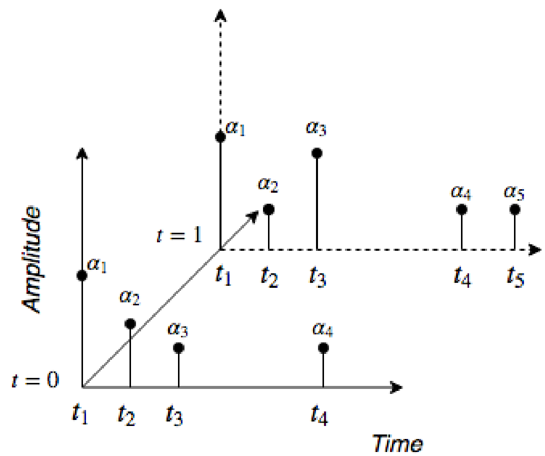

Figure 3.6: Impulse response for a time and frequency selective channel

3.3 Noise

The additive white Gaussian noise (AWGN) channel is the most widely used channel in wireless communication field. This model usually assumes that the signal is adding zero-mean noise having a Gaussian distribution. If the samples of the noise process are uncorrelated with each other over the bandwidth of our interest, then we say the noise is white. Thus, we get the autocorrelation function given by:

$$R_N(t) = \frac{N_0}{2}\delta(t) \tag{3.13}$$

where $\delta(t)$ is the Dirac delta function and its power spectral density across the frequency range $-\infty < f < \infty$ is constant:

$$S_N(f) = \frac{N_0}{2} \quad \text{watts/Hz} \tag{3.14}$$

Additive noise typically originates from one of two physical processes in receivers:

- Thermal (or Johnson) noise due to random motion of charge carriers in metals or lossy elements

- Shot noise, due to the randomness of charge flow in semiconductors

Then, we have $N_0 = kT_{sys}$ where k is Boltzmann's constant 1.38×10^{-23} and T_{sys} is system noise temperature. The noise power measured in a bandwidth B Hz is

$$P_N = kT_{sys}B \quad \text{watts} \tag{3.15}$$

Thus, we have the dimensionless Signal to Noise ratio (SNR) at the receiver in a bandwidth B Hz is

$$\text{SNR} = \frac{P_r}{kT_{sys}B} \tag{3.16}$$

Chapter 4

Timing Synchronization in OFDM

Synchronization is an important task in all wireless communication receivers. The receiver needs a precise timing synchronization to accurately operate following procedures like data processing and decision making.

This chapter will discuss several ways at synchronization and their pros and cons. The frequency synchronization will be mentioned also, but not in detail since it will be found in my colleagues' work [20]. The comparisons among different synchronization methods will be discussed in the next simulation and results chapter.

4.1 Synchronization using cyclic prefix

This synchronization method is also called Sandell's method in this thesis since it was proposed by Sandell and Beek [13] and is possible whenever a cyclic prefix exists. Timing and frequency estimation are derived from the joint likelihood function which contains the information of both offsets. The joint likelihood function reaches to a peak value when at the arrival time of each OFDM symbol due to the redundant information from cyclic prefix in an OFDM system. Hence, this method is also called maximum likelihood (ML) estimation method.

From Chapter 2 we've seen that the OFDM systems have the structure of Figure 2.11.

There are N-parallel subcarriers which give us N-parallel data subcarriers after IDFT, and then we copy the last L samples of the data as cyclic prefix to the beginning of these N samples to get a complete OFDM symbol with length $N + L$ samples.

Assume the transmitted signal $s(k)$ is in non-dispersive channel with additive complex white Gaussian noise (AWGN) $n(k)$. At the receiver, the arrival time of an OFDM frame (usually consisting of several consecutive OFDM symbols) and the received carrier frequency are both uncertain. The first uncertainty is due to propagation delay and is modeled as a delay in channel response $\delta(k-\theta)$ where θ is the integer-valued index of unknown arriving time of one symbol. The second uncertainty is not only due to local oscillators' differences between the transmitter and the receiver but also due to Doppler shift caused by motions of any terminals, and such uncertainty is modeled as a complex multiplicative distortion with a factor $e^{j2\pi\varepsilon k/N}$ of the received data, where $\varepsilon = \Delta fT$ is the normalized carrier offset between the transmitter and receiver[13]. Therefore, the received data is given by [13] with time index θ and carrier frequency offset ε:

$$r(k) = s(k-\theta)e^{j2\pi\varepsilon k/N} + n(k) \tag{4.1}$$

From Figure 2.9, we've seen that without cyclic prefix, the data coming out of IDFT should be approximately a complex Gaussian distribution with a large number of subcarriers. However, with the insertion of cyclic prefix, the total $N + L$ samples are not white anymore since the cyclic prefix produces to non-zero correlation between some samples. Therefore, the received signal $r(k)$ contains information about θ and ε.

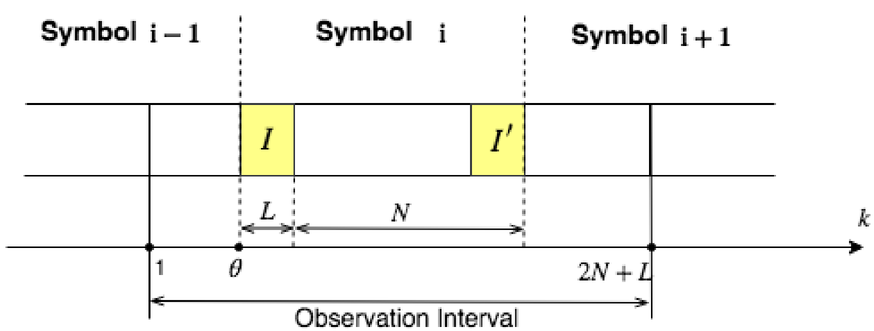

Figure 4.1: Observation of length $2N + L$ samples for a complete OFDM symbol with CP

To obtain the information about θ and ε we need to observe one complete OFDM symbol. Thus, we should observe $2N + L$ consecutive samples to make sure we get one complete OFDM symbol as in Fig 4.1. Since the unknown arrival time index θ is also the beginning of an OFDM symbol, index sets $I = \theta, ..., \theta + L - 1$ denotes the positions of cyclic prefix and index sets $I' = \theta + N, ..., \theta + N + L - 1$ refers the locations of origins of the cyclic prefix. The data placed in these two index sets are strongly correlated. In other words, the samples in cyclic prefix and their copies $r(k), k \in I \cup I'$ are pairwise-correlated [13], i.e. for $\forall k \in I$,

$$E[r(k) \cdot r^*(k+m)] = \begin{cases} \sigma_s^2 + \sigma_n^2, & m = 0 \\ \sigma_s^2 e^{-j2\pi\varepsilon}, & m = N \\ 0 & \text{otherwise} \end{cases} \tag{4.2}$$

while the remaining samples $r(k), k \notin I \cup I'$ are mutually uncorrelated.

Then we can obtain $\Lambda(\theta, \varepsilon)$ which is logarithm of the probability density function $f(\mathbf{r}|\theta, \varepsilon)$ for θ and ϵ. The maximum of this log-likelihood function gives us the estimation of θ and also indicates the correct ε. From [13], we have the following equations:

$$\begin{aligned} \Lambda(\theta, \varepsilon) &= \log f(\mathbf{r}|\theta, \varepsilon) \\ &= \log \left(\prod_{k \in I} f(r(k), r(k+N)|\theta, \varepsilon) \prod_{k \notin I \cup I'} f(r(k)|\theta, \varepsilon) \right) \\ &= \log \left(\prod_{k \in I} \frac{f(r(k), r(k+N)|\theta, \varepsilon)}{f(r(k)|\theta, \varepsilon) + f(r(k+N)|\theta, \varepsilon)} \cdot \prod_{k \in all} f(r(k)|\theta, \varepsilon) \right) \end{aligned} \tag{4.3}$$

where $f(\cdot)$ denotes the probability density function of the variables in its argument. After simplifications, we will get

$$\Lambda(\theta, \varepsilon) = \sum_{k=\theta}^{\theta+L-1} \left(2\mathrm{Re}[r(k) r^*(k+N) e^{j2\pi\varepsilon}] - \rho(|r(k)|^2 + |r(k+N)|^2) \right) \tag{4.4}$$

where

$$\rho = \frac{\sigma_s^2}{\sigma_s^2 + \sigma_n^2} \tag{4.5}$$

By finding the maximum of $\Lambda(\theta, \varepsilon)$ in two steps explained in [13], we obtain ML-estimation of timing index $\hat{\theta}$ from

$$\hat{\theta} = \arg\max_{\theta} \lambda(\theta) \tag{4.6}$$

where

$$\lambda(\theta) = 2\Big|\sum_{k=\theta}^{\theta+L-1} r(k)r^*(k+N)\Big| - \rho \sum_{k=\theta}^{\theta+L-1} \Big(|r(k)|^2 + |r(k+N)|^2\Big) \tag{4.7}$$

and frequency offset estimation $\hat{\varepsilon}$ simultaneously:

$$\hat{\varepsilon} = -\frac{1}{2\pi}\angle\Big(\sum_{k=\hat{\theta}}^{\hat{\theta}+L-1} r(k)r^*(k+N)\Big) \tag{4.8}$$

Thus, we have the estimation of both timing and frequency in the receiver. Since the CP only constitutes a small fraction of the whole symbol, it's reasonable to do averaging over consecutive symbols in Sandell's method to get better accuracy. In this thesis, we are doing 2 consecutive symbol averaging all the time. Figure 4.2 shows the ML estimation of both timing and frequency with 6 consecutive OFDM symbols after averaging (each has a length of 150) and frequency offset of 1000 Hz.

As we can see, the peak appears at each time a new OFDM symbol coming into the receiver. And correspondingly at the peak position, we get the frequency estimation at the same time. In practice, the index of each peak is the very last sample index of the previous OFDM symbol, thus $\hat{\theta} + 1$ is the starting sample of the new OFDM symbol. A peak-finding algorithm will also be introduced in the next chapter to help specify the correct peak position.

4.2 Synchronization using training symbols

This method was first presented by Schmidl and Cox in 1997, [14], and thus is also called Schmidl-Cox method. The start of frame and frequency offset can be detected by using just one training sequence of two consecutive symbols. Note that one frame may contain hundreds of symbols and each symbol contains $N + L$ samples, using one training sequence can only give us one start of a frame which is different from Sandell's method giving us start timing index for each symbol.

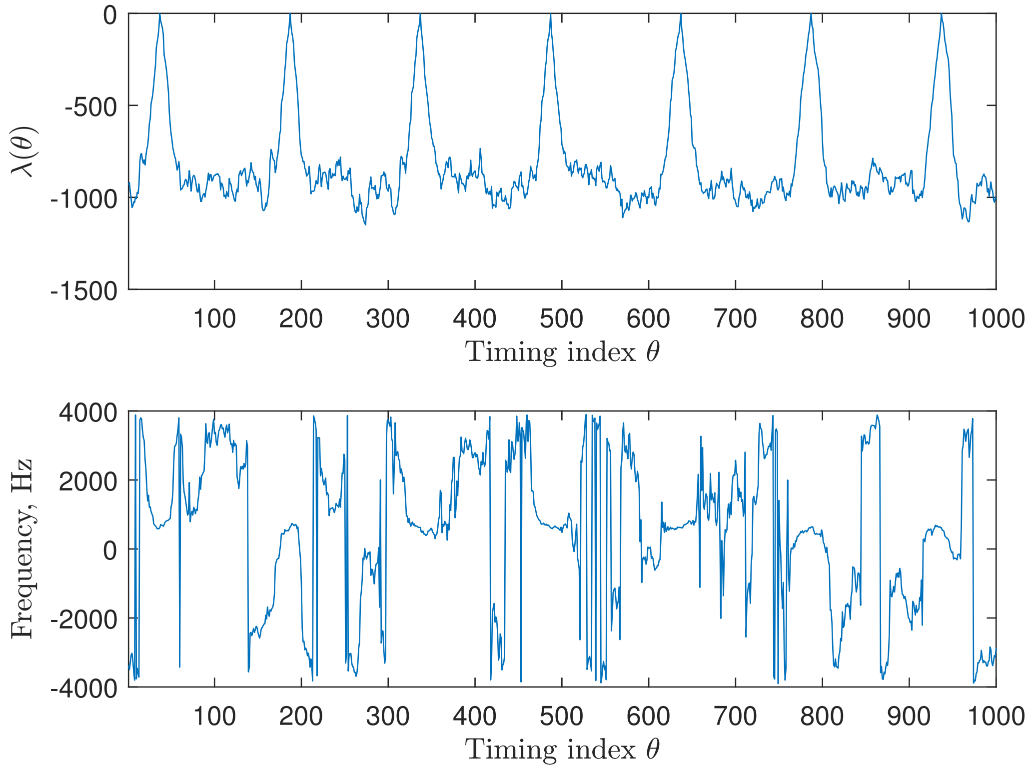

Figure 4.2: Timing and frequency metrics over AWGN channel

The structure of the training symbols is special. By transmitting a pseudo-noise (PN) sequence, which is a random selection from the signal constellation the OFDM system adopted, on the even frequencies and zeroing-out the odd frequencies in the first training symbol, we will obtain two identical halves of the first training symbol in the time domain. The second training symbol is aiming to help find the total frequency offset when there is large Doppler offset exceeding the maximum frequency estimation limit from the first training symbol. The first training symbol would provide all the timing information we need. The larger frequency estimation by using the second training symbol will be introduced in [20].

In the time domain, we know that the first half and second half are identical in the first training symbol as shown in Fig 4.3 except for a phase shift caused by the frequency offset, so we can obtain the approximate frequency information from the first training symbol. Besides, the sum of products of each pair of sample from the first half and corresponding sample in second half will be a large value which gives us timing information. Suppose we want to keep all OFDM

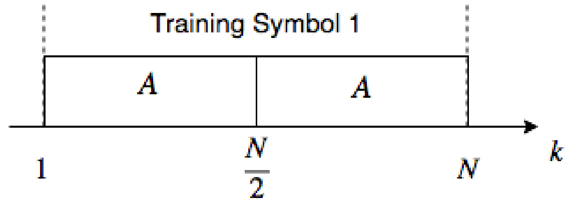

Figure 4.3: Time-domain structure for the first Schmidl-Cox training symbol

symbols have the same length N before inserting cyclic prefix, then there will be $N/2$ complex samples in one-half of the first training symbol before CP insertion. Thus, the sum of the pairs of products is given by [14]:

$$P(d) = \sum_{m=0}^{\frac{N}{2}-1} (r^*(d+m)r(d+m+\frac{N}{2})) \tag{4.9}$$

where d is a time index corresponding to the first sample in a sliding window of N samples. The received energy for the second half-symbol is defined by [14]:

$$R(d) = \sum_{m=0}^{\frac{N}{2}-1} |r(d+m+\frac{N}{2})|^2 \tag{4.10}$$

Then, using $R(d)$ as part of automatic gain control compensation, we will get the timing metric versus time as:

$$M(d) = \frac{|P(d)|^2}{R(d)^2} \tag{4.11}$$

Thus, we get Fig 4.4 on the condition of AWGN channel for OFDM signal with 128 sub-carriers. The position where the maximum value shows up is the timing index for the start of the frame. In Fig 4.4 we can find the timing metric reaches a plateau which has a length of CP (22) near the peak value. This might cause one or two indices' timing estimation error in the receiver. In the next section, Minn's algorithm is trying to avoid the plateau.

The approximate frequency estimation will be made after we find the timing index from

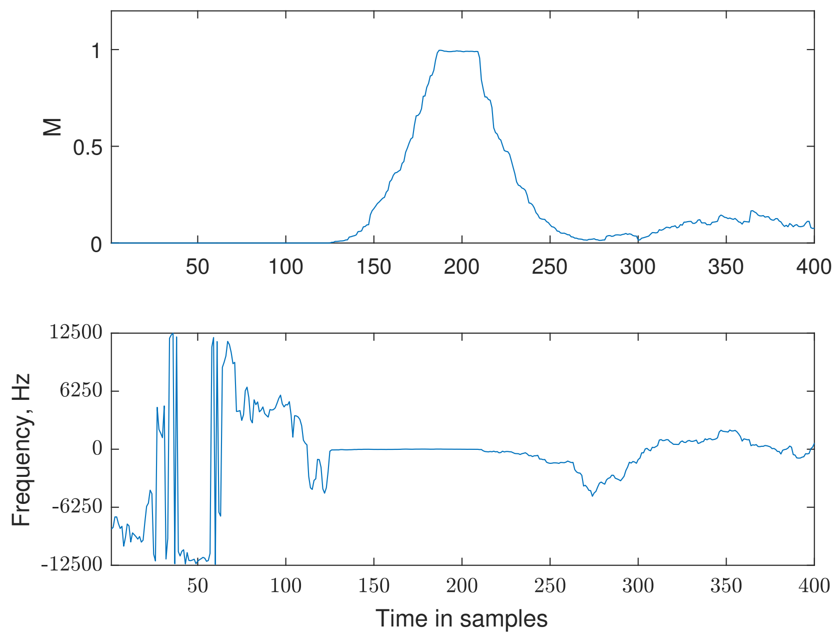

Figure 4.4: Timing metric and frequency estimation using Schmidl-Cox method

$P(d)$:

$$\Delta\hat{f} = \frac{\angle P(d)}{\pi T} \tag{4.12}$$

where T is the duration of one-half symbol time. Figure 4.4 also shows that during the plateau time, the approximate frequency estimation is almost unchanged. If the true frequency offset is not bigger than $\pm 1/T$, which is called tone spacing, we don't need the second training symbol to estimate frequency offset. The second training symbol would not make the frequency estimation error smaller if the true frequency offset is within the tone spacing. However, the second training symbol might provide better channel estimation by sending out a known sequence from the transmitter.

4.2.1 Slight modification of Schmidl-Cox method

- **Sharp peak**: The plateau derived from the timing metric has a length of CP, which is caused by the repetition between CP and its origin. One of the easiest ways to avoid the plateau is adding CP for all other symbols in the OFDM frame except the first training symbol. This is handy to implement, and in this thesis, we use this modification for all results from Schmidl-Cox method. Thus, we have Fig 4.5 which gives us a sharp peak.

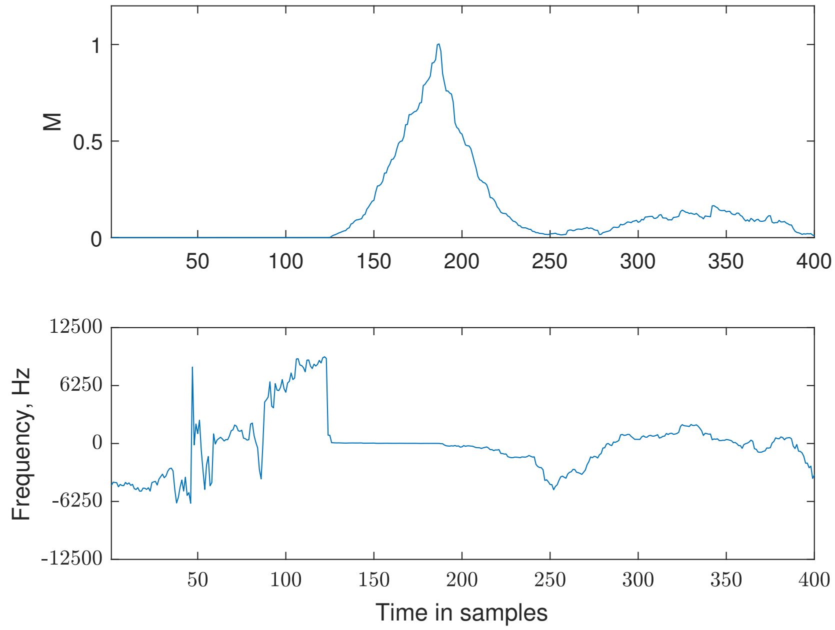

Figure 4.5: Timing metric and frequency estimation using modified Schmidl-Cox method

- **Normalization**: As we can observe from (4.11), we normalized the timing metric by $R(d)$. This introduces a simulation problem which may occur in the practical world: there are $\frac{N}{2}$ samples difference between $P(d)$ and $R(d)$. At the very end of the frame when only noise enters the receiver, $R(d)$ approaches zero before $P(d)$ which in (4.11) gives us a large $M(d)$ at the end. Thus, false alarms may occur anytime in gaps between OFDM symbols.

  The way to solve this problem is adding some arbitrary number in the denominator, where the number is approximately several times smaller than $R(d')$ which is obtained from any data samples before the end of a frame. In our simulation, we add 2048 in the denominator which is determined experimentally. Fig 4.6 compares the M metrics with and without adding an arbitrary number in the denominator (note the scale changes). There are two consecutive OFDM frames shown in the figure. Some silence samples between OFDM frames are also transmitted and received as noise samples only. As we can see, adding the arbitrary number help we suppress the wrong sharp peaks caused by small value noise samples from the end of each OFDM frames. The bottom figure shows strong wrong peaks which make us could not directly see the correct peak with maximum 1 here.

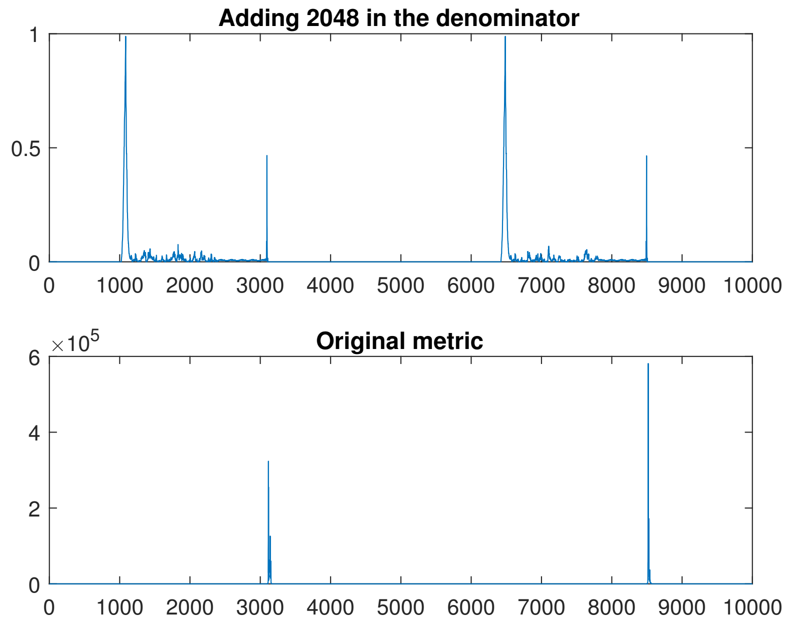

Figure 4.6: Effect of timing metric normalization

4.3 Synchronization using modified training symbols

Minn [15] proposed an improvement on the Schmidl-Cox method to avoid the plateau when finding the timing index. Minn modified the first training symbol to this form before CP insertion:

$$s = [A, A, -A, -A] \tag{4.13}$$

where A are samples of length $N/4$ created by $N/4$-point IFFT of a randomly selected signal from the constellation.

Then (4.9) and (4.10) will be modified into the following forms:

$$P_0(d) = \sum_{k=0}^{1} \sum_{m=0}^{\frac{N}{4}-1} \left(r^*(d + \frac{Nk}{2} + m) \cdot r(d + \frac{Nk}{2} + m + \frac{N}{4}) \right) \tag{4.14}$$

and

$$R_0(d) = \sum_{k=0}^{1} \sum_{m=0}^{\frac{N}{4}-1} \left| r(d + \frac{Nk}{2} + m + \frac{N}{4}) \right|^2 \tag{4.15}$$

The timing metric stays unchanged as

$$M_0(d) = \frac{|P_0(d)|^2}{R_0(d)^2} \tag{4.16}$$

The frequency estimation part in the first training symbol is the same as in Schmidl-Cox [14] method. Figure 4.7 shows the timing metric under high SNR case. As we can see from the figure, Minn's method gives us a sharp peak at the correct timing index (which is also the end index of Schmidl-Cox plateau), but this method has two strong side peaks even in high SNR which may cause false alarm when finding the correct peak, especially when the signal is passing through a noisy channel.

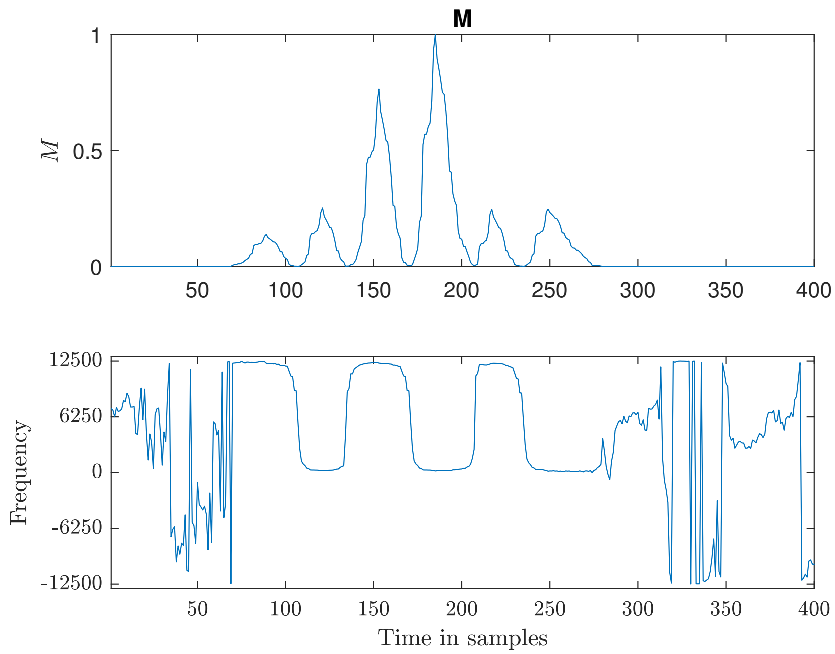

Figure 4.7: Timing metric and frequency estimation using Minn's method

4.4 Synchronization at low SNR using pilot information

During the research of timing and frequency synchronization, we realized the known contribution of pilots can be used to improve the performance of synchronization in Sandell's model [13]. Thus, we proposed a new method to do synchronization using cyclic prefix and pilot carriers together [16].

To make use of the known pilot signal we model the transmitted sample as the superposition of information sample after IFFT, d_n, and pilot sample after IFFT, μ_n:

$$s_n = d_n + \mu_n \tag{4.17}$$

Note that the known pilot sequence is periodic in time with period $N+L$. At the receiver, we measure r_n which delayed version of the signal s_n with additive noise. Then, following the notation of Sandell, we have the log likelihood at timing index N_o given by [16]:

$$\Lambda(N_o) = \log \prod_{m=1}^{M-1} \Big(\prod_{k \in I_1} \frac{f_2(r_{k+m(N+L)}, r_{k+N+m(N+L)}|N_o)}{f_1(r_{k+m(N+L)}|N_o) \cdot f_1(r_{k+N+m(N+L)}|N_o)} \cdot \prod_{other\ \ k} f_1(r_k|N_o) \Big) \tag{4.18}$$

Then we can find the ML estimator of N_o in a single symbol with length of $N+L$ samples by [16]:

$$\begin{aligned}
\hat{N}_o = \arg\max_{N_o} & \underbrace{\sum_{l=N_o+N}^{N_o+N+L-1} \Big\{ 2Re\Big(r_l r_{l-N}^*\Big) - \rho\Big(|r_{l-N}|^2 + |r_l|^2\Big)\Big\}}_{①} \\
& + 2Re\Big\{ (\rho - 1) \underbrace{\sum_{l=N_o+N}^{N_o+N+L-1} r_{l-N}\mu_{l-N_o}^*}_{②} \\
& + (\rho - 1) \underbrace{\sum_{l=N_o+N}^{N_o+N+L-1} r_l^* \mu_{l-N-N_o}}_{③} \\
& + C \underbrace{\sum_{all\ l\ in\ frame} r_l \mu_{l-N_o}^*}_{④} \Big\}
\end{aligned} \tag{4.19}$$

where $C = \frac{\sigma_n^4 + 2\sigma_n^2\sigma_d^2}{\sigma_d^2(\sigma_n^2+\sigma_d^2)} = \frac{1+2\ \mathrm{SNR}}{\mathrm{SNR}^2+\mathrm{SNR}}$, and $\rho = \frac{\sigma_d^2}{\sigma_n^2+\sigma_d^2}$. Note that ②, ③ and ④ can be implemented by three match filters in practice, and the implementation of ① is just similar to Sandell's method. To be consistent with the result from Sandell's method in this thesis, we are also doing two consecutive symbols averaging all the time for our proposed method. Figure 4.9 shows the result of the our method at low SNR with $N = 128$, $P = 11$, $L = 22$ and 3 consecutive symbols.

As we can see from Fig 4.8, we obtain a very sharp peak at the correct timing index when at low SNR while Sandell's method may produce peak index several samples off.

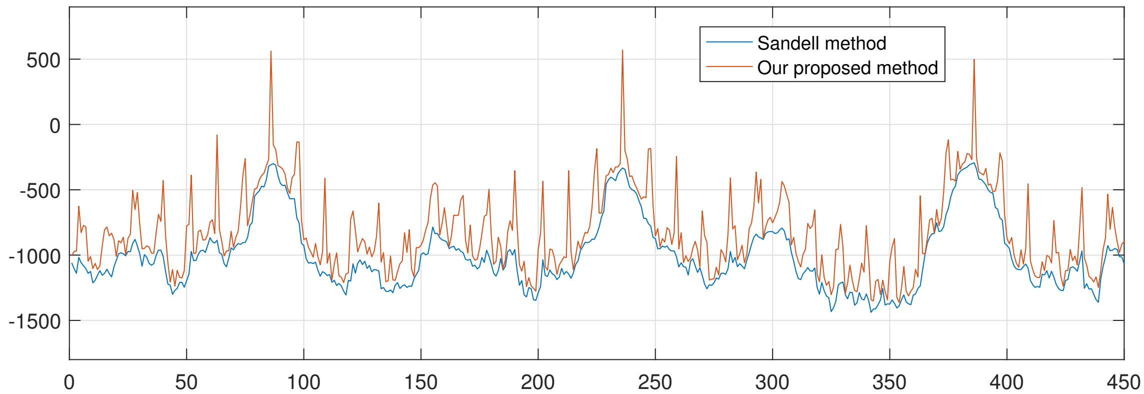

Figure 4.8: Pilots spaced equally

However, if the pilots' position are equally-spaced in one OFDM symbol, as we can see in Fig 4.8, there will be more lower peaks. In this thesis, we recommend equally-spaced pilots shift one or two samples each to the right or left to prevent multiple peaks, and thus making the pilots' positions semi-random. This would help us to avoid the result with multiple small peaks due to the autocorrelation of μ_n, and give us Fig 4.9.

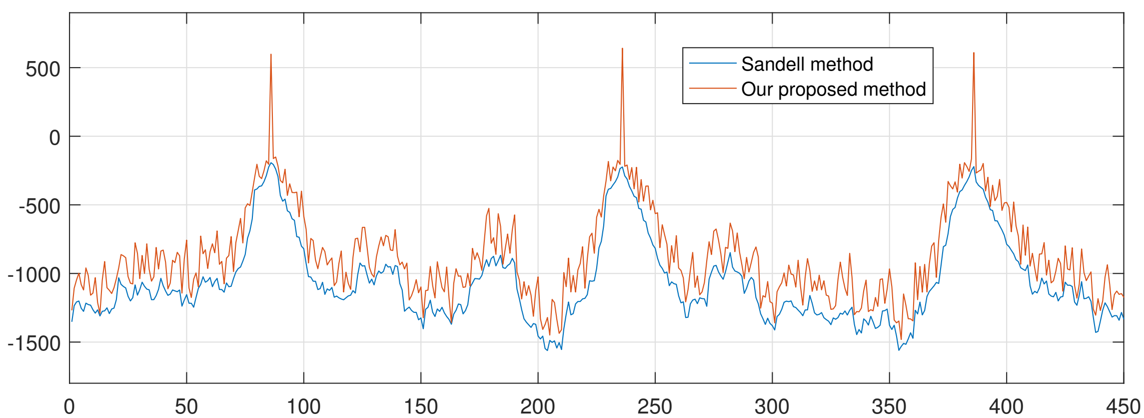

Figure 4.9: Comparison of Sandell's method and our proposed method at 5 dB

Chapter 5

Simulation and Results

In this chapter, we compare the performance of the four timing estimation methods explored in this thesis. The comparison is based on different situations and gives the RMSE plot for each method at the end.

Before going to the simulation results, we first define some of the crucial parameters being used in the simulation in Appendix A. Then we simulated multiple frames containing 282 OFDM symbols.

All simulation results displayed in this chapter are from Mathworks MATLAB®, and MATLAB functions are utilized when available.

5.1 OFDM system parameters

For each OFDM symbol, we are using in the simulation before IFFT and the structure is in Fig 5.1. There are 11 pilots with $\sqrt{2}$ times larger amplitude than data samples' power and carefully-placed in data position. Each symbol contains 8 guard subcarriers on both sides. The DC value in each symbol is also nulled out. After inserting the data samples and doing the IFFT of the whole symbol, CP is added, and the length of the OFDM symbol now is $N + L = 150$.

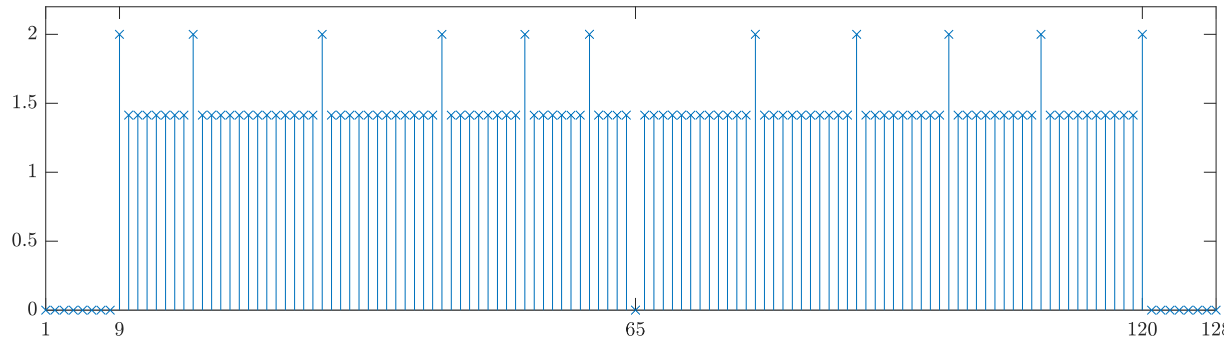

Figure 5.1: One OFDM symbol structure with semi-random pilot locations

5.2 Timing error effects

We've discussed several methods to help us find the correct timing in the previous chapter. Why is synchronization so important? What would happen if we don't get the perfect timing? In this section, we are going to explore the effects of timing error.

It's easy to answer the first question since we can't process the data correctly without timing synchronization. Thus we can't get the original information. That's why it is essential. For the second question, if the timing error is within half CP samples on both sides, we can still get back to original information after compensation in theory. But in our design, we found the limit of our timing synchronization error is 6 samples instead of 11 samples (half of our CP samples). If the timing error is beyond 6 samples, then the system collapse, and we can't get back to the original information. The reason that our project has a timing error limit of 6 samples is because the density of pilots' location which we will explain later.

The primary causes for imperfect timing are:

- Low SNR: When at low SNR like 5 dB, the peak in timing metrics becomes noisy, thus the actual peak may be several samples off the correct peak.
- Multipath: When there is multipath in the transmission, the peak usually is from the strongest path. But with other paths' influencing, the peak could shift several samples to another position.

- Imperfect decimation: We often transmit signal with higher sampling frequency, and then decimate the digital received data to original rate. Since the decimation may start at any random sample at a high rate then decimates periodically from this random sample. The decimated random sample may not be the exact original low rate sample, and it's more likely something between two original consecutive samples. Thus, even at high SNR without multipath, the timing index is correct, but it's still not perfect timing due to imperfection decimation.

Fig 5.2a is the constellation with perfect timing before compensation at high SNR without multipath. There is only some small rotation caused by propagation delay in this situation. Fig 5.2b shows the pilots in the complex axis after compensation. As we can see, all pilots are placing at the same location here. Fig 5.2c shows the constellation with imperfect timing which is 2 samples off the correct timing index in the same situation. From Fig 5.2d we find the pilots are all over the complex plane. This is because the incorrect timing shift produces an increasing phase slope in the received data. The more shift of timing index, the deeper phase slope we get after compensation at pilots' location. Fig 5.2e also shows imperfect timing but with no sample off (meaning only imperfect decimation here). This tells us imperfect decimation means a fraction of one sample timing offset in fact. Fig 5.2g is usually the general case we would meet in practice with imperfect decimation and a small amounts of timing error. Thus, the big ring (or potential ring) across all symbols is due to imperfect timing.

With perfect timing or imperfect timing, we can get back to the original constellation by compensating as shown in 5.3. But with wrong timing (which means large timing error) as in Fig 5.4a, we cannot obtain the original information after compensating as shown in Fig 5.4c. In our research, the limit is 6 samples off since the phase slope between two consecutive pilots is bigger than π when 6 samples off the correct timing index. Thus, we will have a shallow phase compensation instead of very steep phase compensation after unwrapping [21]. The way to solve this problem is by placing denser pilots in each symbol to avoid phase incrementation between pilots goes beyond π. This also reveals that if we want to get back to a perfect constellation, additional constraint on how much time shift can be tolerated is added. Conventionally we can

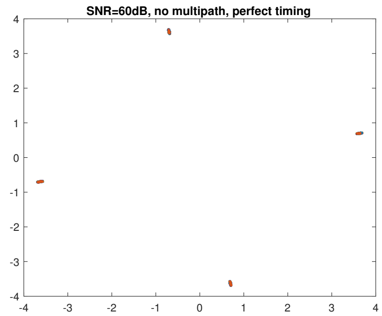

(a) Perfect timing before compensation

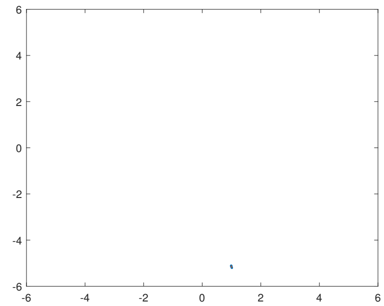

(b) Perfect timing pilots

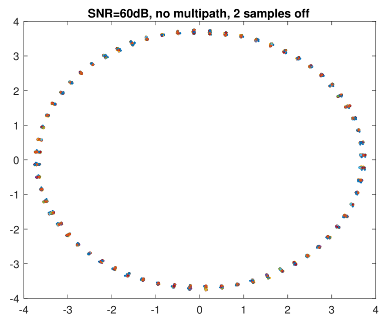

(c) 2 samples off before compensation

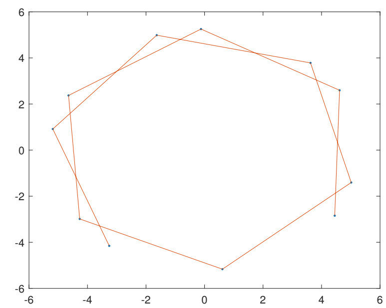

(d) 2 samples off timing pilots

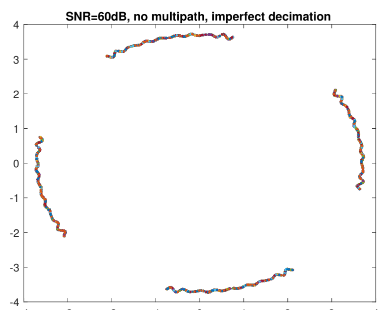

(e) Imperfect decimation before compensation

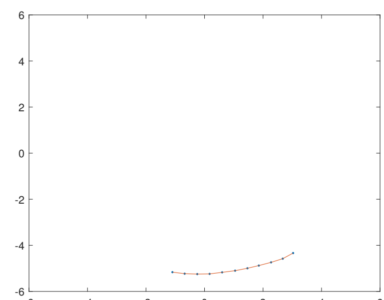

(f) Imperfect timing pilots

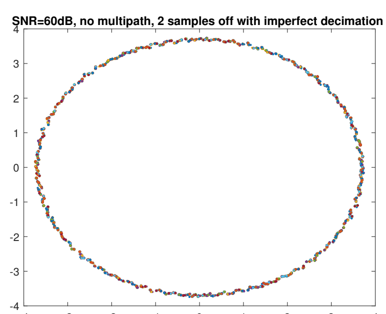

(g) 2 samples off with imperfect decimation

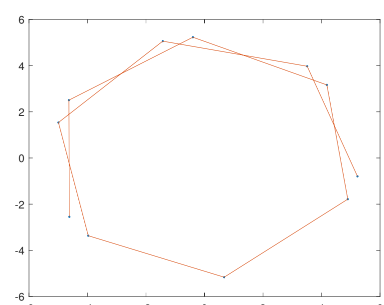

(h) 2 samples off timing with imperfect decimation timing pilots

Figure 5.2: Perfect timing and imperfect timing constellations

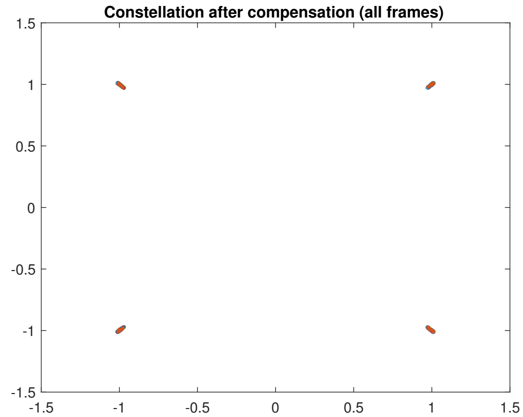

Figure 5.3: Constellation after compensation

shift ± half the CP length under ideal decimation on an ideal channel, but the pilot spacing in frequency domain also enters the picture.

5.3 QPSK timing results comparison

Now we compare the timing results of Sandell's, Schmidl-Cox' and our proposed method from the same incoming data for one received protocol frame with 320 OFDM symbols under different conditions. The result of Minn's method is coming from another incoming protocol frame because its training symbol is a modification of Schmidl-Cox' training symbol, and in our simulation, we do not put Schmidl-Cox' and Minn's training symbol together in one protocol frame.

Since we are modeling high-speed aircraft transmission in our simulation, the influence of different SNR, multipath and Doppler shift are significant. In the following subsections, we will compare different methods in case of SNR, multipath and Doppler shift.

5.3.1 Results at different SNR

Fig 5.5a and Fig 5.5b are the comparisons between high SNR, which is 30 dB, and low SNR, which is 5 dB for Sandell's method. The peak value of the timing index is marked with the red cross, and the correct timing index is marked by θ in each figure. As we can see from Fig 5.5b, the

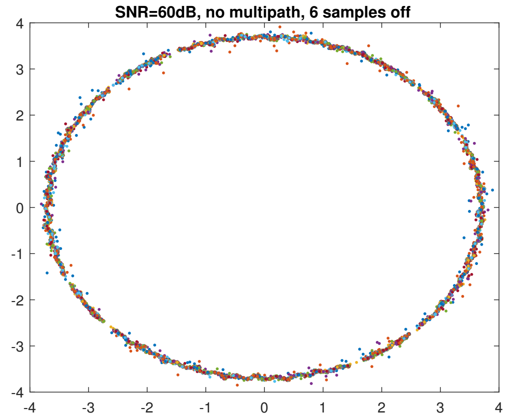

(a) 6 samples off before compensation

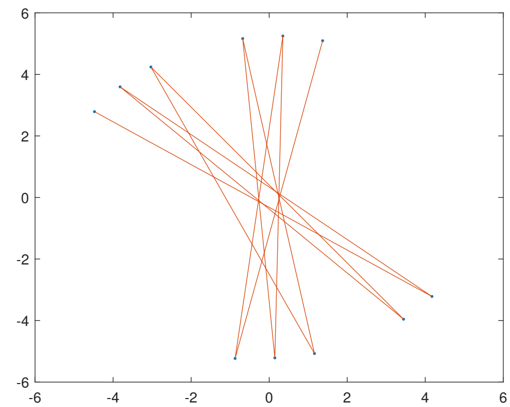

(b) 6 samples off timing pilots

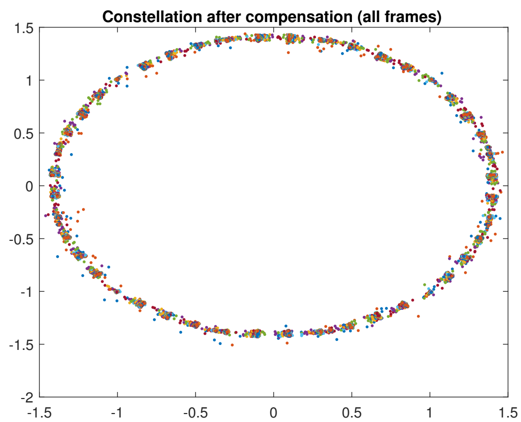

(c) 6 samples off after compensation

Figure 5.4: Wrong timing constellation after compensation

actual third timing index is 1 sample off the correct timing index. Fig 5.5c and Fig 5.5d are the timing indices distributions for one frame, modulo the symbol length 150. From the figures, the distributions become more scattered at low SNR than at high SNR.

Next, we compare the performance of our proposed method for QPSK at the same situation above.

Then, we compare the performance of the Schmidl-Cox' method at different SNR. As we can see from Fig 5.7b, when it reaches low SNR as 5 dB, the peak value drops from 1 to approximately 0.8, and it sometimes gives us a timing index shifted by 1 sample.

Now we compare the performance of Minn's method at different SNR. Since it is a modified

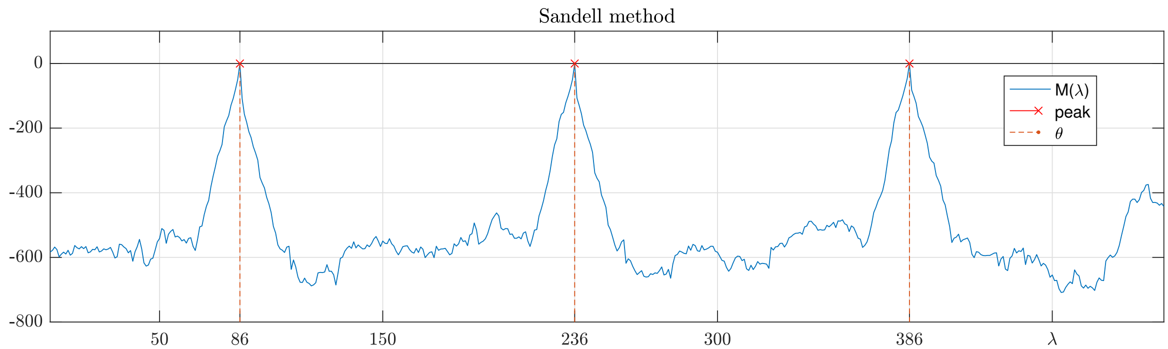

(a) 3 consecutive OFDM symbols at 30 dB

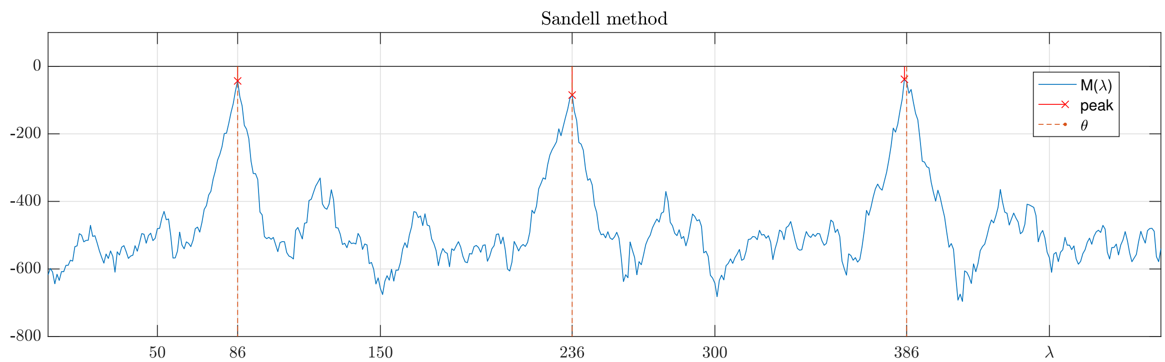

(b) 3 consecutive OFDM symbols at 5 dB

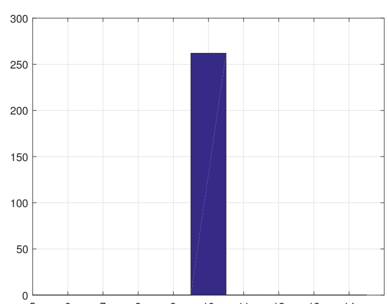

(c) Distribution at 30 dB

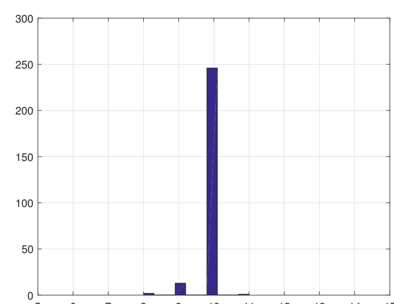

(d) Distribution at 5 dB

Figure 5.5: Comparison for Sandell's method at different SNR

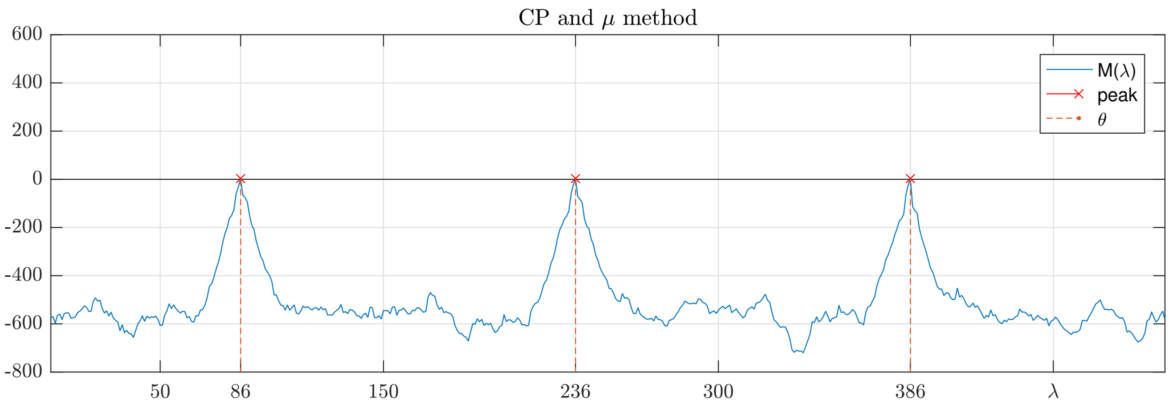

(a) 3 consecutive OFDM symbols at 30 dB

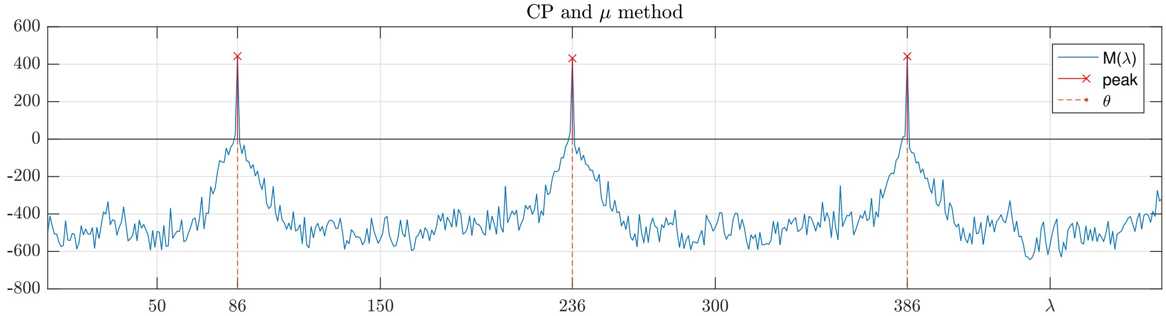

(b) 3 consecutive OFDM symbols at 5 dB

Figure 5.6: Comparison for our proposed method at different SNR

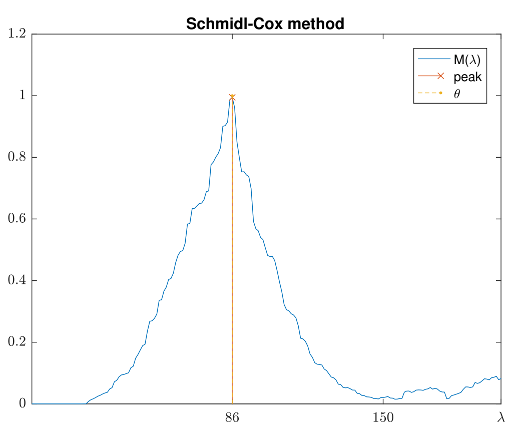

(a) OFDM training symbol at 30 dB

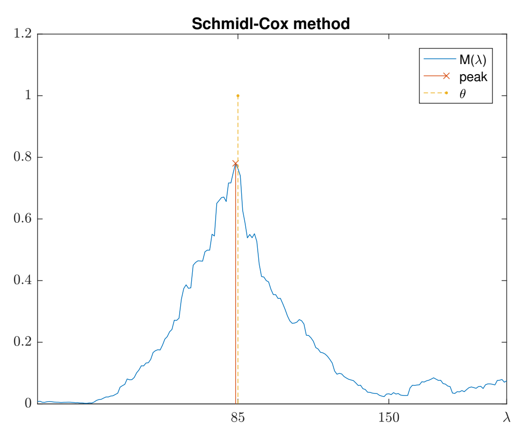

(b) OFDM training symbol at 5 dB

Figure 5.7: Comparison for Schmidl-Cox' method at different SNR

version of Schmidl-Cox method, we can find the peak value drops at low SNR as in Schmidl-Cox. The timing index sometimes also shift 1 or 2 samples at low SNR but not shown in Fig 5.8b.

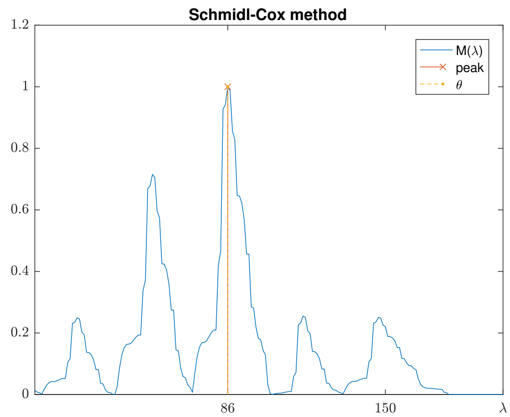

(a) OFDM modified training symbol at 30 dB

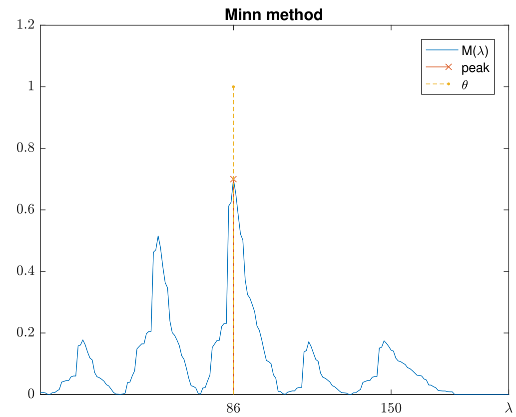

(b) OFDM modified training at 5 dB

Figure 5.8: Comparison for Minn's method at different SNR

5.3.2 Results with multipath

Suppose we have two paths with path gain 0.9, 0.4 and at same low SNR, 5 dB. Fig 5.9 gives us the comparison. We can first compare them with the figures at 5 dB SNR in the previous subsection. The peak becomes flatter in multipath than in single path, which also gives us more timing offsets here. In Fig 5.9a which is Sandell's method, there are three peaks: the first one has 2 samples offset in timing, and the third one has 1 sample offset. In Fig 5.9b, we can see 2 sharp peaks in each symbol. This also shows another benefit in our proposed method which is at low SNR when there is multipath, it could give us multiple peaks in each frame corresponding to the individual path gain and also the interval between these peaks reveal the approximately delay spread. Its potential to identify multipath and path gain at low SNR may be helpful in OFDM data processing.

In Fig 5.9c and Fig 5.9c, it happens to give us the correct timing index. However, we may still get more timing offsets in the multipath than the single path. This assumption will be proved in the next section with RMSE vs. SNR plot.

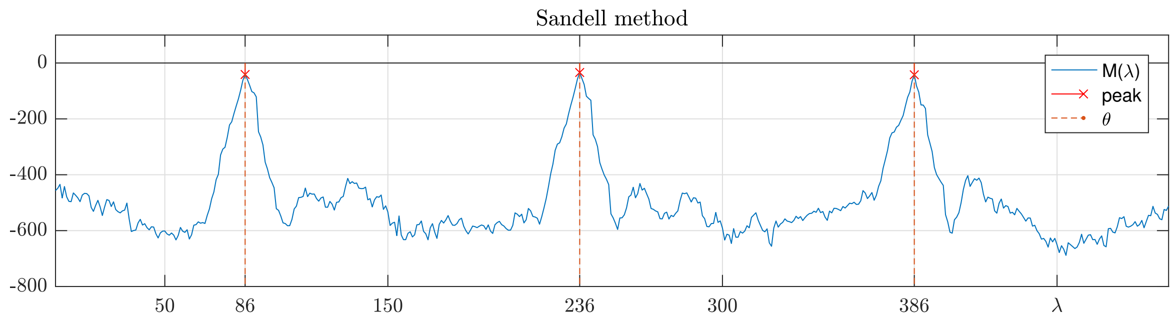

(a) Sandell's method

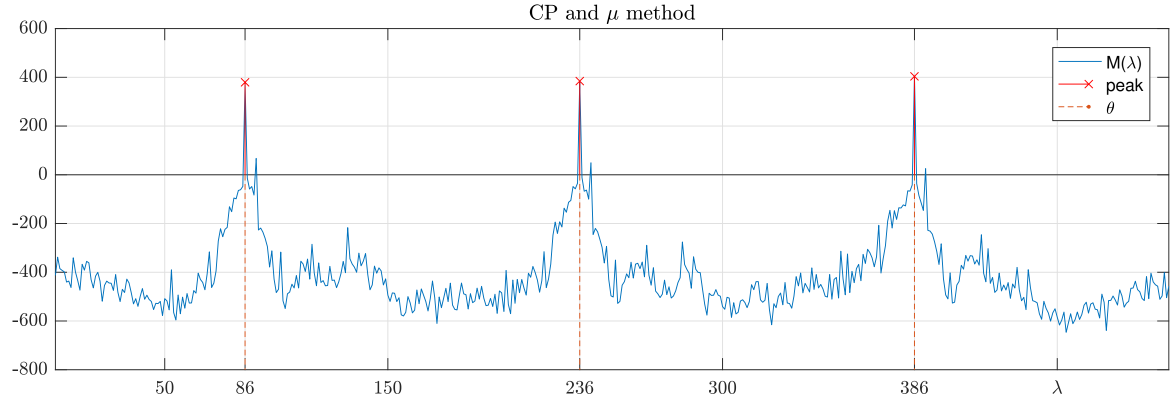

(b) Our proposed method

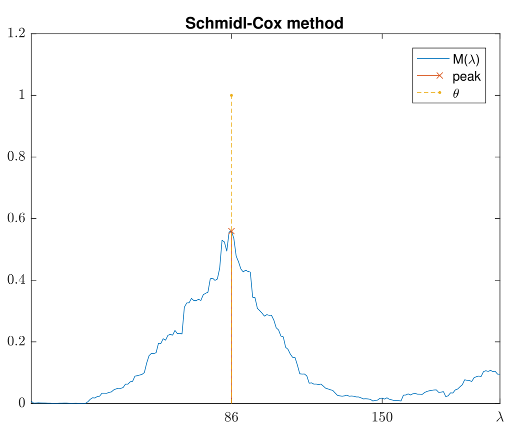

(c) Schimidl-Cox' method

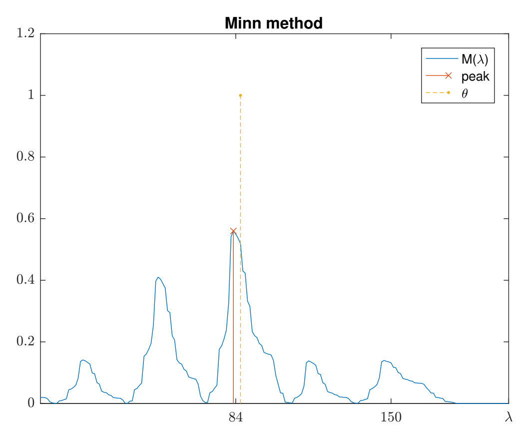

(d) Minn's method

Figure 5.9: Multipath results with different methods at 5 dB

5.3.3 Results with Doppler offset

Another important effect for high-speed aircraft is large Doppler offsets modulating to the received signal. Note that our proposed method is based on known frequency offset, so the method won't appear in Doppler shift comparison.

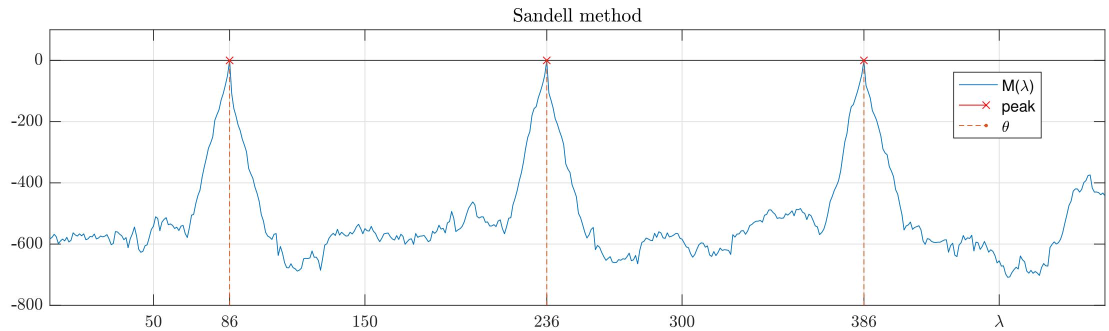

(a) Sandell's method

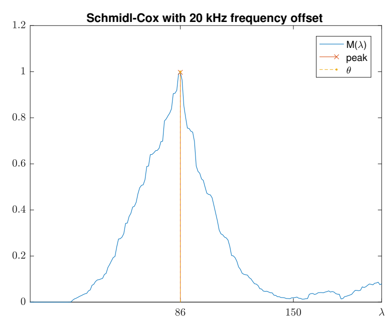

(b) Schmidl-Cox' method

Figure 5.10: Timing results with Doppler offset

No matter how large the Doppler offset is, it does not have any influence on finding timing index. From (4.11) and (4.16), we can confirm that Doppler offset doesn't involve in timing finding since the denominator is the sum of absolute value square of complex data and the numerator is the sum of absolute valued of conjugate products of some complex data for Schmidl-Cox' and Minn's metric. In Sandell's metric from (4.7), the result is the sum of the absolute value of conjugate products then subtract the sum of absolute value square. Thus, in both situation, the timing metrics are invariant to frequency offset. Fig 5.10 is using Sandell method and Schmidl-Cox method to find timing index with 20 kHz Dopper offset (which is $v = 1000$ m/s far beyond the maximum velocity of our aircraft speed model). As we can see from the figure, the timing index is still in the same position as in Fig 5.5a and 5.7a.

The major impact on the received signal with the Doppler offset is the frequency estimation becoming more complicated since the true frequency offset may beyond the tone spacing, which is illustrated in [20].

5.4 RMSE of timing index under different SNR

For more general cases, we get the peaks using different methods for multiple times and then find the root-mean-square error (RMSE) under different SNR. In order to get the same amounts of timing indexes and then make the comparison, we are not using the same received signal from one run for different synchronization methods. For Sandell's method and our proposed method, we are running 10 frames which give us 2820 peaks in total for each SNR, but we have discarded the beginning and ending peaks and only grab 2700 peaks in the middle for each SNR. For Schmidl-Cox' method, we are running 100 loops for 27 frames each loop to get 2700 peaks at each SNR. Thus, at each SNR, we are calculating 2700 peaks for the RMSE. Since Minn's method has strong sidelobes in practice which could sometimes trigger false alarms at low SNR, and our modified Schmidl-Cox method has already got a sharp peak, we would not recommend Minn's method in our research project. Thus, there's no RMSE plot for Minn's algorithm in this section.

Fig 5.11 is the log-scale RMSE plot for the single path with different methods. Since our proposed method gets 0 error all the time, we could not directly see the RMSE of our proposed method in the log-scale plot, and it is the best algorithm at present condition. Sandell's method and Schmidl-Cox' method are similar when at higher SNR than 5 dB. When at low SNR, Schmidl-Cox' method is better than Sandell's method.

Fig 5.12 is the log-scale RMSE plot for multipath. Here we adopt a multipath system with 2 paths, and the path gains are 0.8 and 0.6 in the channel. As we can see from the Fig 5.12, compared with Fig 5.11, all three methods approach a floor due to multipath. Schmidl-Cox has stable performance, while Sandell's method performs the worst. Our proposed method is pretty

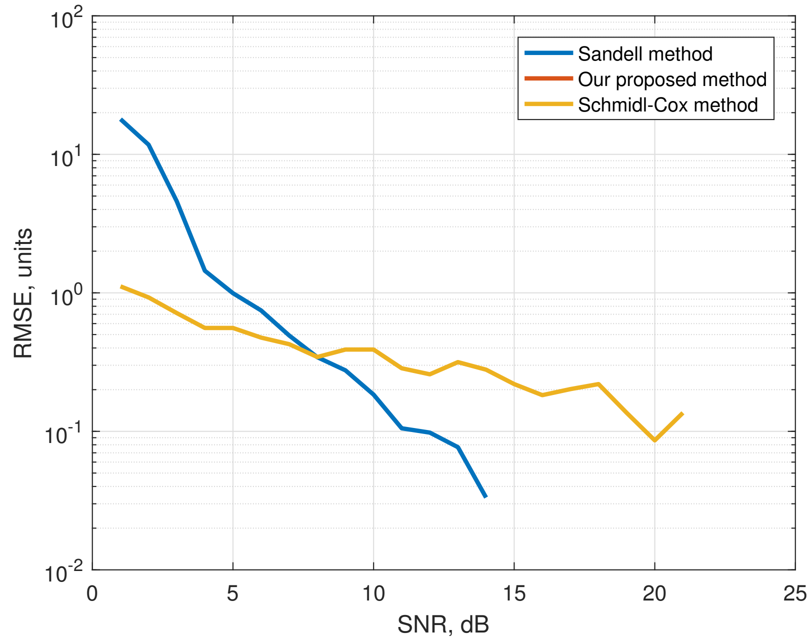

Figure 5.11: RMSE for different methods with single path

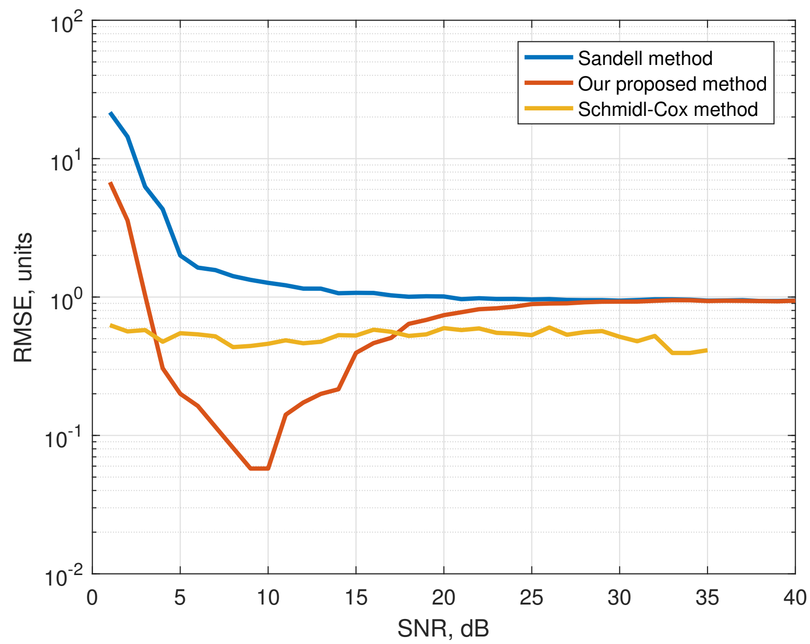

Figure 5.12: RMSE for different methods with two-ray multipath

good at low SNR, but due to the coefficient related to SNR (4.19), the performance is dragged to Sandell's performance at high SNR. Thus, our proposed method is the best at low SNR, while Schmidl-Cox' method is the best at high SNR.

We made a brief test to check consistency of the Sandell estimator by averaging timing estimates over eight symbols, rather than two. Results are shown in Fig 5.13, and indeed we see an expected improvement with averaging length. This is evidence, though not a proof, of consistency of averaged Sandell estimates. This improvement grows as long as the true timing index does not change with symbol position in the sequence.

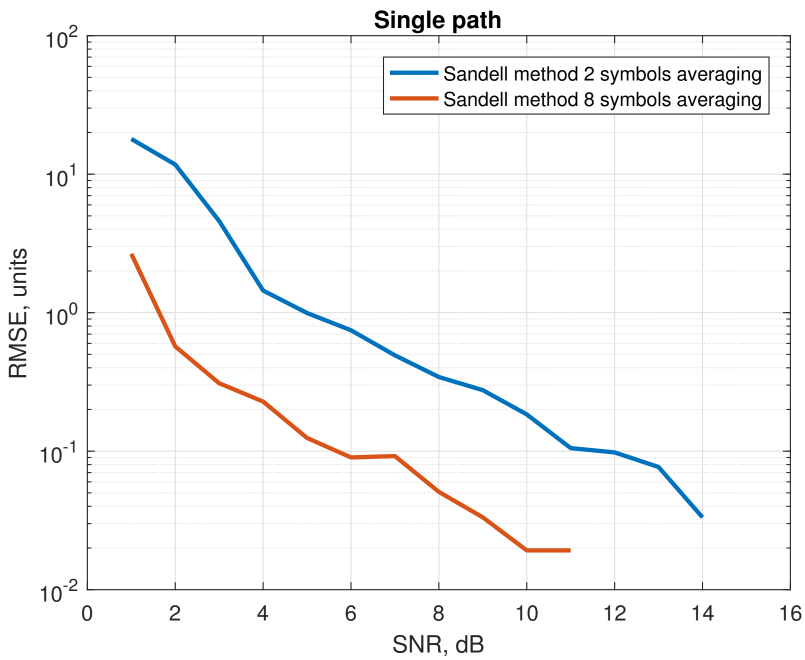

Figure 5.13: RMSE for different averaging lengths for Sandell's method

Chapter 6

Conclusion

In this thesis, we discussed four different synchronization models under various conditions for an airborne OFDM system. Then we compare Sandell's, Schmidl-Cox' and our proposed method by a RMSE versus SNR plot. The results show that if the phase shift (or frequency offset) is known to the receiver, our proposed method has the best performance at low SNR with different path models. If the phase shift is unknown to the receiver, our proposed method could not be used while Schmidl-Cox' method seems to be very stable and reliable at low SNR. However, we need two more training symbols in each frame design for Schmidl-Cox' method. Sandell's method makes the use of each OFDM symbol and produces smaller RMSE when at high SNR, but it gets a larger RMSE when at low SNR. Minn's algorithm is not listed in the RMSE plot due to its strong side peaks which may affect choosing the right timing index at low SNR or in multipath.

Moreover, since each OFDM frame may have hundreds of symbols, using Schmidl-Cox' training symbol to get timing and frequency information at the beginning may not be enough for a fast changing channel. The performance will degrade at the end of each frame when the frame duration is long and the channel is changing during this period. In such case, Sandell's method shows advantages since it is finding timing and frequency in each symbol.

In addition, the complexity of each method is different. Our proposed method is the most complicated one so far and should under the condition of knowing the phase shift at the receiver. Sandell's method is finding the timing and frequency offset in each symbol, which may consume more power than Schmidl-Cox' and Minn's method. Schmidl-Cox' method may be the least complicated one, but it requires extra training symbols in the OFDM frame design.

In our project design, we decide to use Schmidl-Cox' method to do timing synchronization since it is very reliable and stable at different SNRs in practice. An airborne system may have large propagation delay and multipath effect on the received signals. These effects usually cause the timing synchronization has one or two samples off the correct timing index in Schmidl-Cox' method. However, the system is designed to have a tolerance of 6 samples off the correct timing index. Thus, Schmidl-Cox' method meets our project design requirement.

Future work

First is making comparisons between transmitting QPSK signal and 16QAM signal to see if the conclusion of the synchronization methods in QPSK fits for 16QAM, and also seeing if higher-order modulation is better than QPSK. Then improving the results by comparing different methods with 3 or 4-path channel models at different SNR.

Second is improving our proposed method to make it work with an unknown phase shift. Maybe trace down the RMSE versus SNR plot by finding a mathematical way to prevent it from reaching Sandell's method curve at high SNR.

Appendix A

Overview of project context for research (S.G. Wilson)

This research was sponsored by Laulima Systems, under contract to the National Spectrum Consortium, with the intent of providing enhanced spectral efficiency for Air Force telemetry test ranges, along with opportunities to utilize new, but already assigned C-band spectrum on a non-interference basis. The adopted scheme is to use up to eight OFDM carriers placed on 2 MHz centers across the C-band region, using frequencies chosen to avoid interference with legacy users.

Each OFDM carrier has a clock rate of 1.6 Msps at the output of CP insertion, and with pulse shaping the RF spectrum fits within the 2 MHz interval. The FFT size for each OFDM carrier is 128, giving a tone spacing of 7.8 kHz. Eight guard subcarriers are used on each edge for avoiding channel overlap. With the zero-frequency channel also dropped for reasons of DC offset, and $P = 11$ pilots chosen, the payload consists of 100 active data subcarriers in each OFDM symbol. With QPSK modulation, 200 bits are sent in a symbol duration, including CP of length 22 samples, of 93.75 microseconds, producing a data rate, per carrier, of 2.13 Mbps. With eight OFDM carriers active, the air-to-ground data rate is 17.1 Mbps.

The transmission protocol organizes emissions into frames of duration 30 milliseconds. In each frame we assign 6 OFDM intervals of silence, for differential propagation guard time, 2

Schmidl-Cox start-of-frame symbols, 280 payload symbols, 16 symbols where the aircraft sends probe signals to the base station to measure channel quality over multiple frames, and finally 14 symbols of silence for radio silence to determine channel activity by legacy users on all available channels. Frames repeat on 30 millisecond boundaries. The uncoded throughput per channel is thus 200 bits per symbol, 282 payload symbols per 30 milliseconds, or 1.88 Mbps.

While most of the research and development reported in this thesis is generic to OFDM technology, some of the parameter choices and simulation values are driven by the project design. Moreover the work on handling large Doppler offset, and processing signals with very low SNR are motivated by project demands.

Bibliography

[1] S.B. Weinstein, P.M. Evert, Data Transmission by Frequency Division Multiplexing Using the Discrete Fourier Transform, IEEE Trans. On Commun. Tech., Vol.COM-19, pp.628-634, October 1971

[2] Houman Zarrinkoub. Understanding LTE with MATLAB. MathWorks, Massachusetts, 2013.

[3] OFDM PAPR reduction with linear coding and codeword modification, Aylin Susar, Middle East Technical University, Aug. 2005

[4] R. Chang and R. Gibby, "A Theoretical Study of Performance of an Orthogonal Multiplexing Data Transmission Scheme," in IEEE Transactions on Communication Technology, vol. 16, no. 4, pp. 529-540, August 1968.

[5] B. Hirosaki, "An Orthogonally Multiplexed QAM System Using the Discrete Fourier Transform," in IEEE Transactions on Communications, vol. 29, no. 7, pp. 982-989, July 1981. doi: 10.1109/TCOM.1981.1095093

[6] A. Peled and A. Ruiz, "Frequency domain data transmission using reduced computational complexity algorithms," ICASSP '80. IEEE International Conference on Acoustics, Speech, and Signal Processing, 1980, pp. 964-967.

[7] J. A. C. Bingham, "Multicarrier modulation for data transmission: an idea whose time has come," in IEEE Communications Magazine, vol. 28, no. 5, pp. 5-14, May 1990. doi: 10.1109/35.54342

[8] R. W. Chang, "Synthesis of band-limited orthogonal signals for multichannel data transmission," in The Bell System Technical Journal, vol. 45, no. 10, pp. 1775-1796, Dec. 1966.

[9] B. Saltzberg, "Performance of an efficient parallel data transmission system," in IEEE Transactions on Communication Technology, vol. 15, no. 6, pp. 805-811, December 1967.

[10] Tzi-Dar Chuieh, Pei-yun Tsai, OFDM baseband receiver design for wireless communications, 2007, pp 10-54

[11] J.J van de Beek,P. Odling, S.K. Wilson, and P.O. Borjesson Orthogonal Frequency-Division Multiplexing, Synchronizatino and Channel Estimation in OFDM Sytems, Lulea University of Technology, September 1998

[12] A.V. Oppenheim and R.W. Schafer, Digital-Time Signal Processing. Eaglewood Cliffs, NJ: Prentice Hall, 1989

[13] J. J. van de Beek, M. Sandell and P. O. Borjesson, "ML estimation of time and frequency offset in OFDM systems," in IEEE Transactions on Signal Processing, vol. 45, no. 7, pp. 1800-1805, Jul 1997.

[14] T. M. Schmidl and D. C. Cox, "Robust frequency and timing synchronization for OFDM," in IEEE Transactions on Communications, vol. 45, no. 12, pp. 1613-1621, Dec 1997. doi: 10.1109/26.650240

[15] H. Minn, M. Zeng and V. K. Bhargava, "On timing offset estimation for OFDM systems," in IEEE Communications Letters, vol. 4, no. 7, pp. 242-244, July 2000. doi: 10.1109/4234.852929

[16] S. G. Wilson, R. Shang and R. He, "Frame synchronization for OFDM using cyclic prefix and pilot carriers," MILCOM 2017 - 2017 IEEE Military Communications Conference (MILCOM), Baltimore, MD, 2017, pp. 214-218

[17] A. Bahai, B. R. Saltzberg, and M. Ergen, Multi-Carrier Digital Communications: Theory and Applications of OFDM, 2nd ed., New York: Springer Verlag, 2004.

[18] Simon Haykin, Micheal Moher, "Modern Wireless Communications". Upper Saddle River. NJ 07458. 2005. Print

[19] H.T. Friis, "A note on a simple transmission formula". IRE Proc.:254-256,. May 1946.

[20] Ruixuan He, "Frequency offset compensation in OFDM transmission". University of Virginia. July 2018

[21] Mrugen Deshmukh, "Channel estimation in wireless OFDM systems: interpolation versus ESPRIT". University of Virginia. May 2018